RESEARCH ARTICLE

Chemoselective Proteomics, Zinc Fingers, and a Zinc(II) Model for H_2S Mediated Persulfidation

Andrew T. Stoltzfus†[a], Jasper G. Ballot†[b], Thibaut Vignane[c], Haoju Li[a], Madison M. Worth[a], Ludovic Muller[a], Maxime A. Siegler[b], Maureen A. Kane[a], Milos R. Filipovic[c]*, David P. Goldberg[b]*, and Sarah L. J. Michel[a]*

[a] A.T. Stoltzfus, H. Li, M.M. Worth, L. Muller, Dr. M.A. Kane, Dr. S.L.J. Michel
Department of Pharmaceutical Sciences
University of Maryland School of Pharmacy
20 Penn Street, Baltimore, MD, 21201
E-mail: smichel@rx.umaryland.edu

[b] J.G. Ballot, M.A. Siegler, Dr. D.P. Goldberg
Department of Chemistry
Johns Hopkins University
3400 N Charles Street, Baltimore, MD, 21218
E-mail: dpg@jhu.edu

[c] T. Vignane, Dr. Milos Filipovic
Leibniz-Institut für Analytische Wissenschaften –
ISAS - e.V.
Dortmund, Germany, 44139
E-mail: milos.filipovic@isas.de

† These authors contributed equally to this work.

Supporting information and the ORCID identification number(s) for the author(s) for this article is given via a link at the end of the document.

Abstract: The gasotransmitter hydrogen sulfide (H_2S) is thought to be involved in the post-translational modification of cysteine residues to produce reactive persulfides. A persulfide-specific chemoselective proteomics approach with mammalian cells has identified a broad range of zinc finger (ZF) proteins as targets of persulfidation. Parallel studies with isolated ZFs show that persulfidation is mediated by zinc(II), O_2, and H_2S, and intermediates involving oxygen- and sulfur-based radicals were detected by mass spectrometry and optical spectroscopies. A small molecule zinc(II) complex exhibits analogous reactivity with H_2S and O_2, giving a persulfidated product. These data show that zinc(II) is not just a biological structural element, but also plays a critical role in mediating H_2S-dependent persulfidation. ZF persulfidation appears to be a general post-translational modification and a possible conduit for H_2S signaling. This work has broad implications for our understanding of H_2S-mediated signaling and the regulation of ZFs in cellular physiology and development.

Introduction

Hydrogen sulfide (H_2S) was initially identified in the 1770s as a noxious gas present in sewers.[1] It was later determined that H_2S was present on the anoxic, pre-biotic earth, about 3.8 billion years ago, and was involved in the formation of early life (see Figure S1A).[2] In the 1990s, H_2S was discovered to function as an endogenous gasotransmitter, making it the third gasotransmitter after CO and NO.[3] Many biological roles have since been ascribed to H_2S, including neuromodulation, regulation of inflammation, cardiovascular function, metabolism, transcription, and apoptosis.[4] Misregulation of H_2S is associated with inflammatory diseases such as arthritis, cardiovascular disease, and cancer.[5] Although H_2S has been proposed as a key signaling molecule in biology, a molecular level understanding of many of its mechanisms of action remains elusive.

Targets of H_2S include heme and non-heme iron proteins, reactive oxygen-, sulfur-, and nitrogen species, and cysteine residues (see Figure S1B).[1, 6] The interaction of H_2S with cysteine residues, directly and indirectly, can lead to persulfidation, a post-translational modification (PTM) that involves the addition of sulfur to the Cys sulfur terminus (RSH → RSSH).[6c, 7] Evidence over the last two decades suggests that persulfidation by H_2S may be as important a PTM as phosphorylation, and developing a fundamental understanding of H_2S-mediated modifications would be of widespread significance.[1, 3b, 4a, 6c, 6e, 7b]

Zinc finger proteins (ZFs) carry out a myriad of transcriptional and translational roles and are one of the most

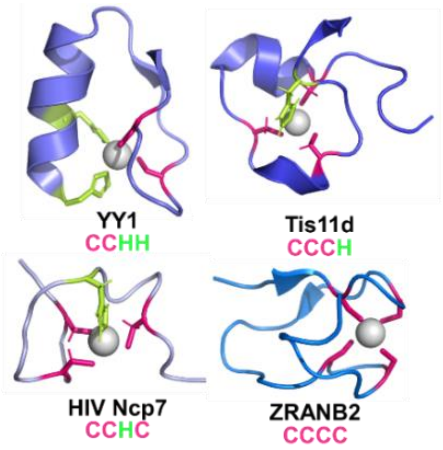

Figure 1. Structures of four different ZF domains/ligand sets; Cys colored pink and His green (made in PyMol, PDB: YY1: 1UBD; Tis11d: 1RGO; HIV Ncp7: 2L44; ZRANB2: 3G9Y).

abundant types of cysteine-rich proteins in eukaryotes, making them ideal targets for H_2S signaling through persulfidation.[8] ZFs are comprised of domains with distinct secondary structures that include four-coordinate zinc(II) sites bound by a combination of cysteine (Cys) and histidine (His) residues.[9] Since the discovery of the first type of ZF, which contains two cysteine and two histidine residues (CCHH) that serve as ligands for zinc, at least 30 other types of ZFs have been identified.[8c] Each class or type of ZF is delineated based upon the ligand set, fold, and function. Figure 1 provides examples of four classes of ZFs. The prevailing dogma is that the Zn^{II} centers in ZFs function exclusively as structural cofactors, in keeping with their stable, d^{10} electron configurations and the absence of any biologically relevant redox chemistry.[8b, 10]

There is emerging evidence of persulfidation of cysteine residues in ZFs by H_2S.[11] These data are primarily from cellular studies, and do not involve the direct assessment of the reactivity of isolated and purified ZFs with H_2S. There is a singular study of H_2S reactivity with an isolated by ZF, reported by some of us.[11a] This work was focused on tristetraprolin (TTP) which is a CCCH type ZF protein that regulates inflammation by controlling cytokine mRNA levels in cells.[12] TTP binds to specific sequences in the 3'-UTR that are adenine and uracil rich (AU-rich), forming a protein/RNA complex that is then targeted for degradation. RNA binding by TTP requires the two CCCH domains, with Zn^{II} bound.[9] Given the role of TTP in regulating inflammation, a role also ascribed to H_2S, we sought to determine whether TTP is persulfidated by H_2S. We found evidence for persulfidation of the cysteine residues in TTP, provided that Zn^{II} was bound to TTP and the reaction with H_2S was performed under aerobic conditions. Several intermediates during persulfidation including oxygen- and sulfur-based radical species were identified. The final stage of the reaction involved disulfide bond formation, Zn^{II} ejection, and loss of TTP/RNA binding function.[11a] The data led to a proposed mechanism in which the Zn^{II} cofactor functions as both an organizational element and electron conduit, bringing the Cys target residue, H_2S, and O_2 together for electron transfer and S-S bond formation (see Scheme S1).

Our work on TTP, together with earlier ZF persulfidation studies by others[11b-d, 13] led us to hypothesize that persulfidation of ZFs might be a general PTM, and not simply operative for a singular case of a TTP construct. We now present a chemoselective persulfide-specific proteomics study in multiple eukaryotic cells, a systematic examination of new protein constructs representing different canonical ZFs, and a novel small-molecule synthetic ZF analog.

Results and Discussion

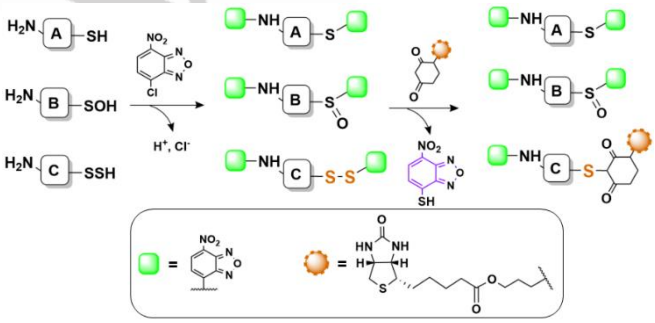

Scheme 1. Dimedone-switch labeling of cellular persulfides for proteomics analysis.

Zinc Finger Proteins are Broadly Persulfidated in Multiple Mammalian Cell Lines

The ZF proteome in MEF was determined using deep proteome analysis. 5927 proteins were found in four biological replicates (see Table S1); of these proteins, 471 (8%) were identified as ZFs. ZFs make up 8-10% of eukaryotic proteomes, and these results are in line with this prediction.[8a, 14] A persulfide specific cell labeling strategy that utilizes a dimedone probe to identify protein persulfides (Scheme 1)[15] revealed that 2435 proteins were persulfidated (see Table S1), of which 118 were ZFs. The ZFs were grouped based upon the ligand sets: CCCC, CCCH/CCHC and CCHH, corresponding to different types of ZFs. The most frequent ligand set found among persulfidated ZFs was CCCC (44%), followed by CCCH/CCHC (38%) and CCHH (18%) (Figure 2; see also Table S2) indicating that the ZFs with more cysteine residues are persulfidated more frequently. Alternative persulfide specific proteomics methods have been applied to

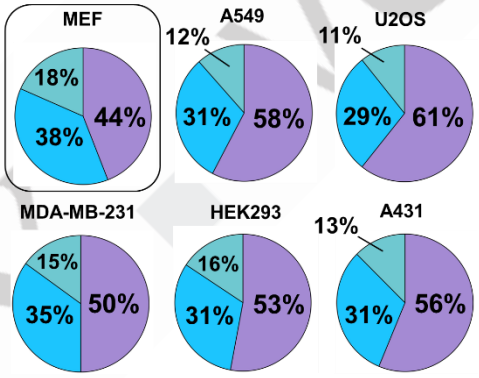

Figure 2. Distribution of persulfidated ZF in different cell types, sorted by ZF ligand set: CCCC (purple), CCCH or CCHC (blue), and CCHH (cyan).

other cell types, and we analyzed the available data from five different human cell lines (A431, A549, U2OS, HEK293, MDA-MB-231) to determine the robustness and generality of our proteomics findings.[16] ZFs were identified in all cell lines evaluated, and a strikingly similar pattern for the frequency of persulfidation emerges: CCCC (44-61%), CCCH/CCHC (29-38%) and CCHH (11-18%) (see Figure 2 and Table S2). This analysis reveals that ZF protein persulfidation occurs for a variety of ZFs in a wide range of cells from human to mouse. To our knowledge, broad persulfidation of ZFs in mammalian cells has not been

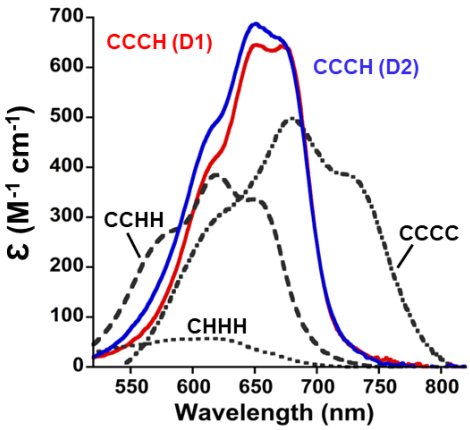

Figure 3. UV-visible spectra from 520 to 820 nm of the apo-ZF peptides upon addition of 1 equivalent of $CoCl_2$ (50 mM HEPES, pH 7.5).

documented up to now. This has potentially far-reaching implications, suggesting that persulfidation of ZFs is a common, if not essential, mode of transport for H_2S signaling in eukaryotes.

H_2S Reactivity of Zinc Fingers with CCCC, CCCH, CCHH and CHHH ligand sets

The persulfide specific proteomics data revealed that a variety of ZFs can be persulfidated. ZFs can be differentiated into different classes based upon their ligand set, their structure or their function. The H_2S reactivity of isolated ZF peptides with varied ligand sets (CCCC, CCCH, CCHH) was examined to determine if persulfidation of ZF sites, as seen via proteomics, occurs at the protein level. ZF domains are modular, allowing for the isolation of single peptide domains that bind Zn^{II} and fold.[9, 17] ZF variants were prepared based upon TTP, which contains two CCCH ZF domains and for which a single domain (TTP-D1) has been previously isolated.[18] Three ZF variants were prepared: TTP-D1-CCCC, D1-CCHH and D1-CHHH, as well as ZF domain 2 (D2-CCCH) (for AA sequences, see Table S3). The CCCC and CCHH variants are native ZF ligand sets whereas CHHH is an abiological derivative.[9, 10] All ZF peptides were isolated in the apo-form and Zn^{II} binding affinities were measured using competitive UV-visible titrations with Co^{II} (Figure 3 and Table 1i; see also Figure S2 and Table S4).[18, 19] Circular dichroism and intrinsic tyrosine fluorescence experiments showed that the ZF peptides form stable complexes with varying degrees of secondary structure (see Table 1ii; see also Figures S3, S4).

Table 1. (i) Upper limit Zn^{II} binding affinities (K_d) for TTP peptides obtained from Co/Zn competitive titrations and (ii) observed change in fluorescence, as fold increase, for direct titrations of TTP variants with Zn^{II}.

TTP Peptide	(i) Zn^{II} K_d (M) [a]	(ii) Fluorescence Fold Increase [a]
D2-CCCH	$1.4 \times 10^{-9} \pm 2.0 \times 10^{-10}$	1.30 ± 0.02
D1-CCCH	$2.1 \times 10^{-9} \pm 2.8 \times 10^{-10}$	1.37 ± 0.02
D1-CCCC	$2.7 \times 10^{-9} \pm 5.0 \times 10^{-10}$	1.11 ± 0.01
D1-CCHH	$1.6 \times 10^{-10} \pm 1.7 \times 10^{-11}$	1.14 ± 0.01
D1-CHHH	$3.1 \times 10^{-7} \pm 1.5 \times 10^{-7}$	1.01 ± 0.01

[a] Numbers following the ± are S.E.M. from replicate experiments (N=3)

The dimedone switch method utilized for the persulfide specific proteomics screen was adapted to detect persulfidation in situ during the reaction of the ZF peptides with H_2S (see Figure S5A).[15a] NBF-Cl was added to each Zn-TTP peptide variant in the presence of O_2 and H_2S and the optical spectra was monitored (Figure 4A, *left*; see also Figure S5B). The NBF-Cl signal at 350 nm decreased with a concomitant increase in absorbance bands

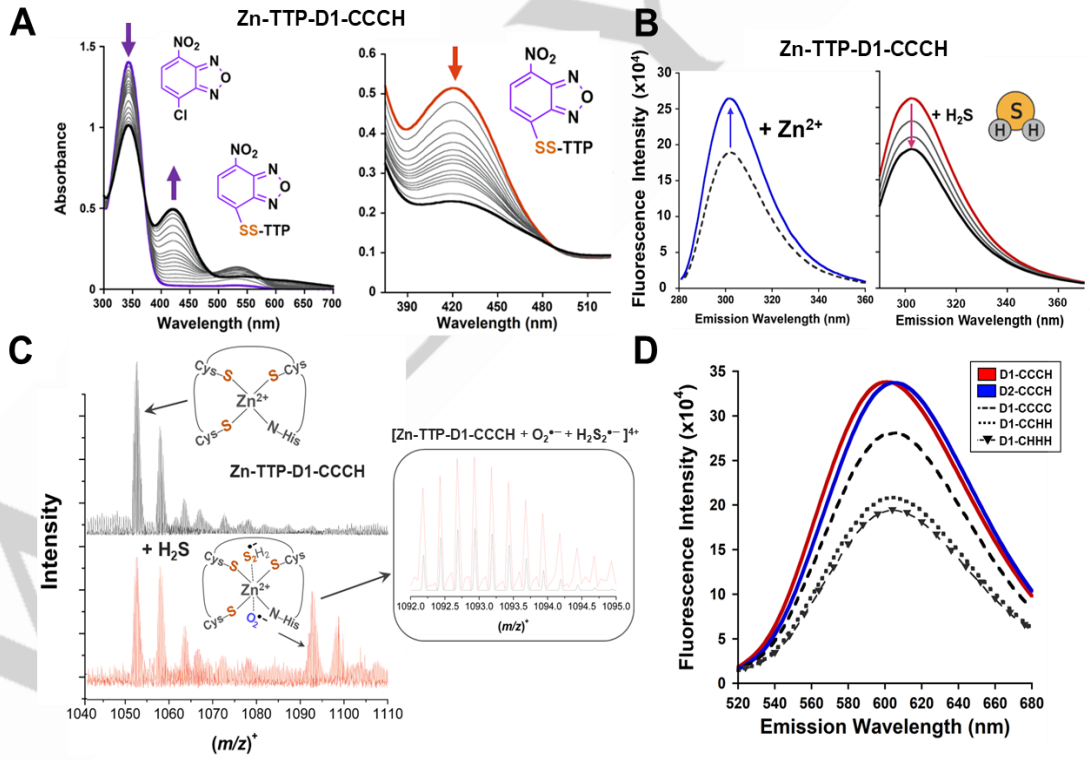

Figure 4. A) UV-Visible spectra of Zn-TTP-D1-CCCH reacted with Na_2S in 100 mM HEPES, pH 7.5. *Left:* plot of spectrum between 300-700 nm after exposure to O_2 and addition of NBF-Cl (purple), followed by the spectra obtained every 30s (grey traces) until no further spectral changes observed (black). *Right:* plot of spectrum between 375-525 nm following addition of dimedone to the same reaction mixture (red), followed by the spectra obtained every 30s (grey traces) until no further change observed (black). B) Plot of the change in the intrinsic tyrosine fluorescence spectrum as apo-TTP-D1-CCCH is bound with Zn^{II} (dashed black to solid blue trace, left) and reacted aerobically with H_2S over 30 minutes (red to black trace, right). C) CSI-MS spectra of the z = 4+ species of Zn-TTP-D1-CCCH (40 µM) in 20 mM NH_4HCO_3 (pH 7.4), before (upper panel) and after (middle panel) addition of 400 µM Na_2S under aerobic conditions. *Inset:* simulated (blue) and experimental (red) spectra overlaid for the intermediate species observed at 1092 *m/z*. D) Fluorescence emission spectra of oxidized hydroethidine after the reaction of ZF peptides with H_2S (aerobic, t= 120 minutes, 50 mM sodium phosphate, pH 7.5).

between 400 to 480 nm as the NBF labeled thiols, amines, sulfenic acids, and persulfide groups.[20] NBF labeling of persulfides forms a mixed disulfide in which one sulfur has enhanced electrophilicity, making it uniquely positioned to react with nucleophilic dimedone (the switch). Reaction with dimedone results in a decrease in the unique wavelength attributed to TTP-SS-NBF (422 nm).[20, 21] This switch was observed upon addition of dimedone to all Zn-TTP peptides (Figure 4A, *right*; see also Figure S5C), supporting persulfidation with a variety of ZF ligand sets. To our knowledge this is the first time that this approach has been employed to trap persulfide intermediates generated in situ, and has the potential inform on persulfidation in other systems.[15a]

Intrinsic tyrosine fluorescence was performed on the TTP-D1- and D2-CCCH peptides to determine the effects of H_2S reactivity on ZF structure. The Zn^{II} bound peptides exhibited a fluorescence emission at 303 nm that diminished upon addition of H_2S under aerobic conditions. This suggests that persulfidation leads to protein unfolding (Figure 4B). Cryo-ESI-MS (CSI-MS), a low temperature, high-resolution mass spectrometric technique that allows for detection of native, metallated peptides and possible adducts with intermediate species, was performed on the TTP-D1-CCCH and -CCCC peptides. Adducts of peptide, superoxide ($O_2^{\bullet-}$), and dihydrogen disulfide radical anion ($H_2S_2^{\bullet-}$), were observed (Figure 4C), akin to what was previously observed for a two domain CCCH ZF construct (TTP-2D).[11a] In the case of D1-CCCH, this radical species was formed immediately upon mixing and could be observed within the first 5 minutes of recording. Some amounts of $[(TTP)(O_2^{\bullet-})(H_2S_2^{\bullet-})]$ were also observed when the CCCC variant was mixed with H_2S, but thiol oxidation and demetallation predominated in the same time frame suggesting that the CCCC ZF's reaction with H_2S may be faster than the CCCH ZF (see also Figure S6).

To detect the superoxide intermediates and understand the effect of ligand set, hydroethidine (HE) was utilized as a probe for superoxide anion (see Figure S7A).[22] The ZF peptides were reacted with H_2S in the presence of O_2 and HE and the change in fluorescence was monitored (emission λ = 520-680 nm; excitation λ = 466 nm). A fluorescence signal developed over time for all ZF peptides (Figure 4D; see also Figure S8) indicating the oxidation of HE by superoxide to products with greater fluorescence intensity.[23] These spectra featured peaks with λ_{max} (~595 nm) which is comparable to that of a control experiment with the xanthine/xanthine oxidase (XOD) enzyme-substrate system, which generates $O_2^{\bullet-}$; HE is oxidized by $O_2^{\bullet-}$ to form the superoxide-specific product 2-OH-E^+ (see Figure S7B).[23] Comparison of the HE signal that formed after 120 minutes between the ZF peptides revealed that the TTP-D1- and -D2-CCCH peptides, which have the native ligand set, exhibited the largest change in fluorescence signal, indicating the generation of the greatest superoxide yields (see Table S5). Additional experiments with hydroethidine and potassium superoxide (KO_2) in solvent systems of either (a) DMSO (aprotic), or (b) potassium phosphate buffer (protic) confirmed the blue-shifted fluorescence of superoxide-specific oxidation vs the red-shifted fluorescence (λ_{max} ~ 630 nm) of non-specific HE oxidation (see Figure S7C). Taken together, the data for the ZF peptides align with the previously proposed mechanism for the persulfidation of Zn-TTP-2D, which involves reduction of oxygen to form $O_2^{\bullet-}$ (see Scheme S1).

Oxygen-dependent Persulfidation of a Synthetic N_2S-Zn^{II} Complex

The results obtained for the ZF peptides indicate that Cys persulfidation results from a Zn^{II}-mediated reaction with H_2S as the sulfur donor and O_2 as the oxidant. Such a reaction has not been previously reported for a biological zinc(II) center, and we wanted to determine if a synthetic, sulfur-ligated Zn^{II} complex with a similar coordination environment could exhibit the same reactivity. The structurally well-defined Zn(PATH)Br (**1**) (PATH = 2-methyl-1-[methyl-(2-pyridin-2-yl-ethyl)amino]propane-2-thiol)[24] provides a Zn^{II} center with a biomimetic N_2S(alkylthiolate) coordination environment and a single thiolato donor, simplifying the analysis for persulfidated product. Complex **1** reacts with SH^- salts to give the new Zn(PATH)(SH) (**2**) as colorless crystals suitable for X-ray structure determination (Figure 5C; see also Table S6). The crystal structure reveals a pseudotetrahedral Zn^{II} complex in which the bromide ligand of **1** has been replaced by a terminal hydrosulfide group. To our knowledge, **2** is the first

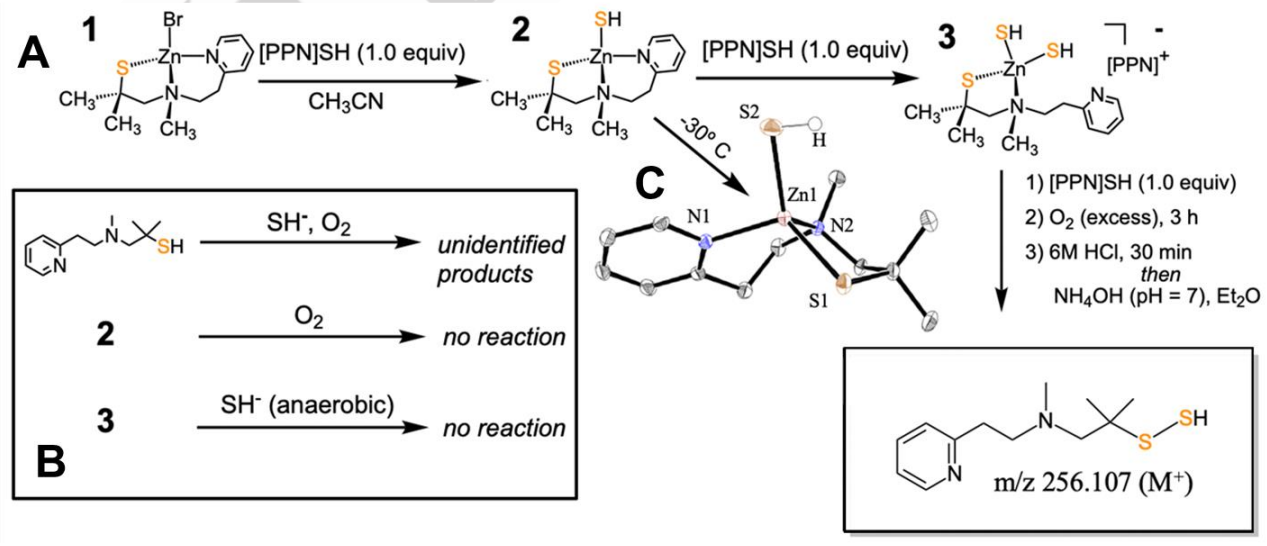

Figure 5. A) Synthesis of complexes 2 and 3, and persulfidation reaction with O_2. B) Control reactions between free ligand PATH, $[(PPh_3)_2N][SH]$ and O_2 (top), 2 and O_2 (middle), 3 and $[(PPh_3)_2N][SH]$ under anaerobic conditions (bottom), showing no formation of persulfide product in each case. C) Displacement ellipsoid plot (50% probability level) of 2 at 110(2) K. Hydrogen atoms (except for S-H) are omitted for clarity.

example of a Zn^{II} complex with both a terminal SH^- and a thiolato group in the first coordination sphere. The structure of **2** is also notable in that little steric protection of the SH^- group is provided to prevent Zn-S(H)-Zn bridged structures, as opposed to the few other isolable, mononuclear $Zn^{II}(SH)$ complexes.[1, 25] The ^1H nuclear magnetic resonance (NMR) spectrum of **2** versus starting material **1** (see Figure S9) shows significant differences, including two new singlets at 1.47 and 1.25 ppm, which are assigned to the diastereotopic, geminal methyl substituents. A new upfield resonance at -1.9 ppm can also be seen for **2**, corresponding to the terminal SH^- group.[25b] The ^1H-NMR data confirm that the crystal structure of **2** remains intact in solution.

Complex **2** was surprisingly inert to O_2, but we hypothesized that addition of excess SH^- might lead to enhanced reactivity, and possibly persulfidation. This idea was based on the proposed mechanism for the persulfidation of TTP, which includes a Zn^{II}-$H_2S_2^{\bullet-}$ intermediate as shown in (see Scheme S1). Addition of 1 equivalent of $[(PPh_3)_2N][SH]$ to **2** under anaerobic conditions in CD_3CN leads to a ^1H-NMR spectrum consistent with displacement of the pyridine arm by SH^-. Analysis of the reaction mixture by FTIR spectroscopy reveals that the vibrational mode for the coordinated pyridyl group (1607 cm^{-1}) shifts to that seen for the free ligand (1587 cm^{-1})(see Figure S10).[26] Together the NMR and IR data indicate that the pyridyl donor has been displaced by a second equivalent of SH^-, leading to $[Zn(PATH)(SH)_2]^-$ (**3**) (Figure 5A; see also Figure S11). This assignment was confirmed by high-resolution ESI-MS (negative ion mode, see Figure S12). This complex is reminiscent of the CCCH-ZF shown in Figure 1, with 3 anionic sulfur ligands and one neutral nitrogen donor.

Unlike complex **2**, the bis(sulfhydryl)-zinc(II) species **3** reacts with O_2, as seen by a gradual color change from colorless to yellow. The addition of an extra equivalent of SH^- to **3** helps push the equilibrium toward complete formation of the bis(SH)-ligated species **3**, and addition of excess O_2 gas under these conditions leads to persulfidation of the PATH ligand (Figure 5A). The persulfidated ligand was identified following demetallation via an acid/base protocol, which resulted in a mixture of persulfidated product together with some free PATH ligand, as seen by ^1H NMR spectroscopy (see Figure S13). The identity of the persulfidated product was confirmed by high-resolution EI-MS ($[M^+]$ = 256.1071 m/z, calculated 256.1067 m/z; see Figure S14), and integration by ^1H-NMR against an internal standard gives a persulfidated yield of 11.8 ± 0.2% (see Figure S15). This relatively modest yield is likely a result of persulfide degradation during work-up; persulfides are well known to be unstable and their isolation is challenging.[1-2, 27] Several control reactions were carried out to determine the requirements for persulfidation, as shown in Figure 5B. The mono-sulfhydryl species **2** is unreactive toward O_2 (see Figure S16) and no persulfidation occurs for the bis(sulfhydryl) species **3** in the absence of O_2 or excess SH^-. Free PATH ligand does not undergo persulfidation, giving instead unidentified products in the presence of excess O_2 and SH^- (see Figure S17). Taken together, these data show that both zinc(II) and O_2 are required for the SH^- mediated persulfidation of the alkylthiolate donor in PATH. This work provides a synthetic example of persulfidation with a Zn^{II}-SR complex, SH^- and O_2.

Conclusion

The modification of cysteine residues to persulfides by H_2S is emerging as an important PTM thought to be connected to signaling by H_2S. This PTM is widely observed, for example, it is estimated that 30% of proteins are persulfidated under resting conditions.[6e, 28] However, the types of proteins that are persulfidated are not well defined, underscoring the importance of identifying proteins that are persulfidated by H_2S. The persulfide specific proteomics data presented here identified cysteine rich ZFs as a type of protein that is widely persulfidated in mammalian cells. Persulfidation occurred for different classes of ZFs (i.e. with different ligand sets), suggesting that ZF persulfidation is broad. This finding challenges the long-held dogma that ZFs use the Zn^{II} center for solely structural purposes. Our investigation of the reactivity of a series of isolated ZF peptides with varied ligand sets as well as with a small synthetic, sulfur-ligated zinc(II) complex with a similar coordination environment as the ZFs, offered further evidence for reactivity at the Zn^{II} center, as well as mechanistic insight. The reaction of ZFs requires O_2, and the data support a mechanism whereby Zn^{II} serves as a conduit for electron transfer between O_2 and HS^-, similar to those proposed for iron and manganese dioxygenases[29] and models of Zn^{II} superoxide dismutase.[30]

A major role for ZFs in biology is to regulate transcription and translation, and a myriad of biological processes rely on this ZF activity. This regulation requires that Zn^{II} is bound to the ZF such that the protein is folded and can directly interact with the DNA or RNA sequence associated with the transcriptional or translational event. The data presented here show that Zn^{II} centers react with H_2S and O_2 to give persulfidated ZFs and metal ion release, suggesting an intriguing new mechanism for transcriptional/translational control.

Supporting Information

The authors have cited additional references within the Supporting Information.[1, 2, 11a, 15a, 16, 19, 23, 24, 31, 32]

Acknowledgements

We thank Prof. Dr. Ivana Ivanovic-Burmazovic, Ludwig-Maximilians-Universität München, Munich, Germany, for use of the ultra-high-resolution cryo-spray-ionization mass spectrometer. S.L.J.M. is grateful to the NIH for funding (R01GM139854). D.P.G. is grateful to the NIH for funding (R35GM149233). Figures were prepared with the following software: Biorender, Kaleidagraph (Synergy software), and ChemDraw (PerkinElmer).

Keywords: zinc finger proteins • proteomics • hydrogen sulfide • small molecules • persulfidation

Entry for the Table of Contents

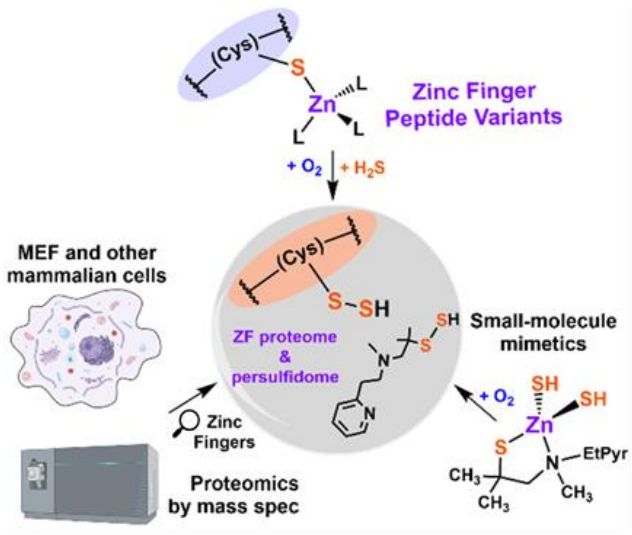

Persulfidation by H_2S is a key modification of proteins. Using persulfide specific proteomics, cysteine rich zinc finger (ZF) proteins were found to be targets of persulfidation. The reaction of H_2S with ZFs was evaluated using a series of ZFs and a small molecule Zn coordination complex that mimics the ZF site. Persulfidation by H_2S occurred in an O_2 dependent manner, with the zinc acting as a conduit for electron transfer and S-S bond formation.

Institute and/or researcher Twitter usernames: @SMichelLab1

References:

[1] M. R. Filipovic, J. Zivanovic, B. Alvarez, R. Banerjee, *Chem. Rev.* **2018**, *118*, 1253-1337.

[2] K. R. Olson, *Free Radic. Biol. Med.* **2019**, *140*, 74-83.

[3] a) R. Hosoki, N. Matsuki, H. Kimura, *Biochem. Biophys. Res. Commun.* **1997**, *237*, 527-531; b) B. D. Paul, S. H. Snyder, *Nat. Rev. Mol. Cell. Biol.* **2012**, *13*, 499-507.

[4] a) B. He, Z. Zhang, Z. Huang, X. Duan, Y. Wang, J. Cao, L. Li, K. He, E. C. Nice, W. He, W. Gao, Z. Shen, *Biochem. Pharmacol.* **2023**, *209*, 115444; b) J. I. Sbodio, S. H. Snyder, B. D. Paul, *Br. J. Pharmacol.* **2019**, *176*, 583-593.

[5] a) E. Donnarumma, R. K. Trivedi, D. J. Lefer, *Compr. Physiol.* **2017**, *7*, 583-602; b) H. Kimura, *Antioxid. Redox Signal.* **2015**, *22*, 362-376.

[6] a) D. Basudhar, L. A. Ridnour, R. Cheng, A. H. Kesarwala, J. Heinecke, D. A. Wink, *Coord. Chem. Rev.* **2016**, *306*, 708-723; b) O. Kabil, R. Banerjee, *Antioxid. Redox Signal.* **2014**, *20*, 770-782; c) J. M. Fukuto, L. J. Ignarro, P. Nagy, D. A. Wink, C. G. Kevil, M. Feelisch, M. M. Cortese-Krott, C. L. Bianco, Y. Kumagai, A. J. Hobbs, J. Lin, T. Ida, T. Akaike, *FEBS Lett.* **2018**, *592*, 2140-2152; d) V. Vitvitsky, J. L. Miljkovic, T. Bostelaar, B. Adhikari, P. K. Yadav, A. K. Steiger, R. Torregrossa, M. D. Pluth, M. Whiteman, R. Banerjee, M. R. Filipovic, *ACS Chem. Biol.* **2018**, *13*, 2300-2307; e) E. Doka, T. Ida, M. Dagnell, Y. Abiko, N. C. Luong, N. Balog, T. Takata, B. Espinosa, A. Nishimura, Q. Cheng, Y. Funato, H. Miki, J. M. Fukuto, J. R. Prigge, E. E. Schmidt, E. S. J. Arner, Y. Kumagai, T. Akaike, P. Nagy, *Sci. Adv.* **2020**, *6*, eaax8358.

[7] a) E. Cuevasanta, M. Lange, J. Bonanata, E. L. Coitino, G. Ferrer-Sueta, M. R. Filipovic, B. Alvarez, *J Biol Chem* **2015**, *290*, 26866-26880; b) B. D. Paul, S. H. Snyder, *Trends Biochem. Sci.* **2015**, *40*, 687-700.

[8] a) C. Andreini, L. Banci, I. Bertini, A. Rosato, *J Proteome Res* **2006**, *5*, 196-201; b) C. Andreini, L. Banci, I. Bertini, A. Rosato, *J. Proteome Res.* **2006**, *5*, 3173-3178; c) K. Ok, M. R. Filipovic, S. L. J. Michel, *Eur. J. Inorg. Chem.* **2021**, *2021*, 3795-3805; d) C. Wiedemann, A. Kumar, A. Lang, O. Ohlenschlager, *Front. Chem.* **2020**, *8*, 280.

[9] S. J. Lee, S. L. Michel, *Acc. Chem. Res.* **2014**, *47*, 2643-2650.

[10] N. J. Pace, E. Weerapana, *Biomolecules* **2014**, *4*, 419-434.

[11] a) M. Lange, K. Ok, G. D. Shimberg, B. Bursac, L. Markó, I. Ivanović‐Burmazović, S. L. J. Michel, M. R. Filipovic, *Angew. Chem. Int. Ed.* **2019**, *131*, 8081-8085; b) K. Zhao, S. Li, L. Wu, C. Lai, G. Yang, *J. Biol. Chem.* **2014**, *289*, 20824-20835; c) C. Du, X. Lin, W. Xu, F. Zheng, J. Cai, J. Yang, Q. Cui, C. Tang, J. Cai, G. Xu, B. Geng, *Antioxid. Redox Signal.* **2019**, *30*, 184-197; d) A. Dey, S. Prabhudesai, Y. Zhang, G. Rao, K. Thirugnanam, M. N. Hossen, S. K. D. Dwivedi, R. Ramchandran, P. Mukherjee, R. Bhattacharya, *Sci. Adv.* **2020**, *6*; e) D. Liu, H. Song, Y. Li, R. Huang, H. Liu, K. Tang, N. Jiao, J. Liu, *Antioxidants* **2023**, *12*.

[12] a) C. Tiedje, M. D. Diaz-Munoz, P. Trulley, H. Ahlfors, K. Laass, P. J. Blackshear, M. Turner, M. Gaestel, *Nucleic Acids Res.* **2016**, *44*, 7418-7440; b) R. Alkallas, L. Fish, H. Goodarzi, H. S. Najafabadi, *Nat. Commun.* **2017**, *8*, 909.

[13] Y. Yuan, L. Zhu, L. Li, J. Liu, Y. Chen, J. Cheng, T. Peng, Y. Lu, *Antioxid. Redox Signal.* **2019**, *31*, 1302-1319.

[14] I. Bertini, L. Decaria, A. Rosato, *J. Biol. Inorg. Chem.* **2010**, *15*, 1071-1078.

[15] a) J. Zivanovic, E. Kouroussis, J. B. Kohl, B. Adhikari, B. Bursac, S. Schott-Roux, D. Petrovic, J. L. Miljkovic, D. Thomas-Lopez, Y. Jung, M. Miler, S. Mitchell, V. Milosevic, J. E. Gomes, M. Benhar, B. Gonzalez-Zorn, I. Ivanovic-Burmazovic, R. Torregrossa, J. R. Mitchell, M. Whiteman, G. Schwarz, S. H. Snyder, B. D. Paul, K. S. Carroll, M. R. Filipovic, *Cell Metab.* **2019**, *30*, 1152-1170 e1113. b) A. Aroca, A. Jurado-Flores, M. R. Filipovic, C. Gotor, L. C. Romero, *Meth. Enzymol.* **2022**, *676*, 385-402

[16] L. Fu, K. Liu, J. He, C. Tian, X. Yu, J. Yang, *Antioxid. Redox Signal.* **2020**, *33*, 1061-1076.

[17] S. Negi, M. Imanishi, M. Hamori, Y. Kawahara-Nakagawa, W. Nomura, K. Kishi, N. Shibata, Y. Sugiura, *J. Biol. Inorg. Chem.* **2023**, *28*, 249-261.

[18] S. L. Michel, A. L. Guerrerio, J. M. Berg, *Biochemistry* **2003**, *42*, 4626-4630.
[19] A. T. Stoltzfus, C. J. Campbell, M. M. Worth, K. Hom, T. L. Stemmler, S. L. J. Michel, *J. Biol. Inorg. Chem.* **2023**, *28*, 85-100.
[20] H. R. P. Ellis, L. B., *Biochemistry* **1997**, *36*, 15013-15018.
[21] a) P. B. Ghosh, M. W. Whitehouse, *Biochem. J.* **1968**, *108*, 155-156; b) V. Gupta, K. S. Carroll, *Biochim. Biophys. Acta.* **2014**, *1840*, 847-875.
[22] M. Hardy, J. Zielonka, H. Karoui, A. Sikora, R. Michalski, R. Podsiadly, M. Lopez, J. Vasquez-Vivar, B. Kalyanaraman, O. Ouari, *Antioxid. Redox Signal.* **2018**, *28*, 1416-1432.
[23] H. Zhao, S. Kalivendi, H. Zhang, J. Joseph, K. Nithipatikom, J. Vásquez-Vivar, B. Kalyanaraman, *Free Radic. Biol. and Med.* **2003**, *34*, 1359-1368.
[24] S. Chang, V. V. Karambelkar, R. C. diTargiani, D. P. Goldberg, *Inorg. Chem.* **2001**, *40*, 194-195.
[25] a) M. D. Hartle, M. Delgado, J. D. Gilbertson, M. D. Pluth, *ChemComm* **2016**, *52*, 7680-7682; b) J. G. Melnick, A. Docrat, G. Parkin, *ChemComm* **2004**, 2870-2871.
[26] U. Brand, H. Vahrenkamp, *Inorganica Chim. Acta* **2000**, *308*, 97-102.
[27] R. A. Hankins, S. I. Suarez, M. A. Kalk, N. M. Green, M. N. Harty, J. C. Lukesh, 3rd, *Angew. Chem. Int. Ed.* **2020**, *59*, 22238-22245.
[28] N. Sen, B. D. Paul, M. M. Gadalla, A. K. Mustafa, T. Sen, R. Xu, S. Kim, S. H. Snyder, *Mol Cell* **2012**, *45*, 13-24.
[29] J. P. Emerson, E. G. Kovaleva, E. R. Farquhar, J. D. Lipscomb, L. Que, Jr., *Proc. Natl. Acad. Sci. U.S.A.* **2008**, *105*, 7347-7352.
[30] M. B. Ward, A. Scheitler, M. Yu, L. Senft, A. S. Zillmann, J. D. Gorden, D. D. Schwartz, I. Ivanovic-Burmazovic, C. R. Goldsmith, *Nat. Chem.* **2018**, *10*, 1207-1212.
[31] G. M. Sheldrick, *Acta. Cryst.* **2015,** 71, 3-8.
[32] B. Kalyanaraman, M. Hardy, R. Podsiadly, G. Cheng, J. Zielonka, *Arch. Biochem. Biophys.* **2017**, *617*, 38-47.

Supporting Information

69451 Weinheim, Germany

Chemoselective Proteomics, Zinc Fingers, and a Zinc(II) Model for H_2S Mediated Persulfidation

Andrew T. Stoltzfus[†], Jasper G. Ballot[†], Thibaut Vignane, Haoju Li, Madison M. Worth, Ludovic Muller, Maxime A. Siegler, Maureen A. Kane, Milos R. Filipovic[*], David P. Goldberg[*], and Sarah L. J. Michel[*]

Abstract: The gasotransmitter hydrogen sulfide (H_2S) is thought to be involved in the post-translational modification of cysteine residues to produce reactive persulfides. A persulfide-specific chemoselective proteomics approach with mammalian cells has identified a broad range of zinc finger (ZF) proteins as targets of persulfidation. Parallel studies with isolated ZFs show that persulfidation is mediated by zinc(II), O_2, and H_2S, and intermediates involving oxygen- and sulfur-based radicals were detected by mass spectrometry and optical spectroscopies. A small molecule zinc(II) complex exhibits analogous reactivity with H_2S and O_2, giving a persulfidated product. These data show that zinc(II) is not just a biological structural element, but also plays a critical role in mediating H_2S-dependent persulfidation. ZF persulfidation appears to be a general post-translational modification and a possible conduit for H_2S signaling. This work has broad implications for our understanding of H_2S-mediated signaling and the regulation of ZFs in cellular physiology and development.

DOI: 10.1002/anie.2021XXXXX

Table of Contents

Table of Contents (continued)

Materials and methods

Materials. Acetonitrile, trifluoroacetic acid (TFA), and Chelex 100 sodium resin were purchased from Sigma. Zinc(II) chloride ($ZnCl_2$), zinc(II) bromide ($ZnBr_2$) cobalt(II) chloride ($CoCl_2$), dithiothreitol (DTT), mono- and di-basic sodium phosphate salts, HEPES (free acid and sodium salt), tris(2-carboxyethyl)phosphine (TCEP), 4-chloro-7-nitrobenzofurazan (NBF-Cl), 5,5-Dimethyl-1,3-cyclohexanedione (dimedone), 1,3,5-trimethoxybenzene, and bis(triphenylphosphine)iminium chloride (PPNCl) were all purchased from Sigma-Aldrich. Zinc(II) acetate ($Zn(OAc)_2$) was purchased from Fluka. Anhydrous sodium sulfide (Na_2S) was purchased from Alfa Aesar. 2-(N-morpholino)ethanesulfonic acid sodium salt (MES) was purchased from VWR. Tris(hydroxymethyl)aminomethane (Tris)-HCl was purchased from Promega. Tris base was purchased from Fisher. 3 kD molecular weight cutoff (MWCO) centrifugal spin-filters (0.2 µM polyethersulfur (PES) membrane) were purchased from Millipore Sigma. Anhydrous sodium hydrosulfide (NaSH) was purchased from Strem Chemicals. All buffers were prepared with Chelex-treated Milli-Q water, filtered through a 0.2 µM PES membrane (VWR), degassed via vacuum purging/N_2-sparging, and stored in a Coy anaerobic chamber (3% H_2 / 97% N_2). $ZnCl_2$, and $CoCl_2$ metal salts were prepared in degassed Chelex-treated Milli-Q water. Acetonitrile and acetonitrile-d_3 were distilled from CaH_2, then degassed by a minimum of three freeze-pump-thaw cycles and stored over freshly activated 3 or 4 Å molecular sieves in the drybox following distillation. The starting ligand (PATH), and starting zinc(II) complex Zn(PATH)Br (**1**), and disulfide $(PATH)_2$ were synthesized and purified according to a literature procedure.[23]

Direct and persulfide specific proteomics of MEF cells. Persulfide-specific proteomics (dimedone switch method) was performed as previously reported.[14b]

Cell culture. Mouse embryonic fibroblast (MEF) cells were grown in Dulbecco's modified Eagle's media (DMEM, high glucose and sodium pyruvate, Gibco™, 21969035) supplemented with 2 mM L-glutamine (Pan Biotech, P04-80100), 1% penicillin-streptomycin (Pan Biotech, P06-07100) and 10% Fetal bovine serum (Sigma Aldrich F9665) at 37°C and 5% CO_2.

Cell lysis (PSSH labeling and enrichment for MS). 80% confluency MEF were lysed in cold HEN Buffer (50 mM HEPES, 1 mM EDTA, 0.1 mM Neocuproine, 1% IGEPAL, 2% SDS, pH 7.4) supplemented with 5 mM 4-Chloro-7-nitrobenzofurazan (NBF-Cl, Sigma, 163260). Cells were scraped and lysates were collected and homogenized using a syringe and needle. Lysates were incubated for 2 hours at 37°C. Proteins were then precipitated twice using methanol/chloroform precipitation and pellets were washed twice with cold methanol.

Samples precleaning and DCP-Bio switch. To reduce unspecific enrichment, samples were cleaned from endogenously biotinylated proteins. Shortly, pellets were resuspended in PBS (Sigma), 0.2% SDS, and protein concentration was performed using DC protein assay (Biorad, 5000112). The same amount of protein was incubated with Pierce™ NeutrAvidin™ Agarose beads (Thermofisher, 29200). After 2 hours of mixing at room temperature (RT), supernatants were collected and precipitated once using methanol/chloroform precipitation. Pellets were suspended in PBS (with 2% SDS) and proteins were incubated for 1.5 hours at 37°C with 250 µM DCP-Bio1 (MERK, NS1226). To remove the excess of DCP-Bio1, proteins were precipitated twice and washed using the same method previously described.

Persulfidation enrichment. After precipitation, pellets were resuspended in PBS 0.1% SDS and protein concentration was performed. The same amount of protein was incubated with Pierce™ High-Capacity Streptavidin Agarose beads (Thermofisher, 20357). After 4 hours of mixing at RT, beads were collected and transferred into Pierce™ Disposable Columns 2 mL (Thermofisher, 29920). To remove unspecific bindings and detergent beads were washed with 28 mL of PBS and 8 mL of water. After washing, enriched proteins were eluted by incubating beads overnight with 2.25 M of ammonia solution (Sigma, 5.33003). After incubation, supernatants were collected and lyophilized.

Protein digestion and peptides desalting. Lyophilized samples were resuspended in digestion buffer (50 mM ammonium bicarbonate, 1 mM calcium chloride). Samples were digested overnight using trypsin (Promega, V5117) at Trypsin: protein ratio 1:20. Samples were then desalted using Supel™-Select HLB SPE Tube (Sigma, 54181-U) following the manufacturer protocol. Shortly, columns were conditioned with the elution solution (60% acetonitrile, 0.1% trifluoroacetic acid (TFA)) and washed twice with washing buffer (0.1% TFA). Each sample was then loaded on the column using gravity flow. Cartridges were washed once with washing buffer by gravity flow followed by two-time gravity flow elution of the peptides using the elution buffer. Eluates were evaporated to dryness.

LC-MS/MS and data analysis (persulfide-specific proteomics). Peptides were dissolved in 0.1% TFA before being analysed by high-resolution LC-MS/MS using an Ultimate 3000 Nano Ultra High-Pressure Chromatography

(UPLC) system coupled with an Orbitrap Eclipse™ Tribrid™ Mass Spectrometer via an EASY-spray (Thermo Fisher Scientific). Peptide separation was carried out with an Acclaim™ PepMap™ 100 C18 column (Thermo) using a 90-minute gradient from 3 to 35% of B (84% acetonitrile, 0.1% formic acid) at a flow rate of 250 nL/min. The Orbitrap Eclipse™ was operated in a DDA mode and MS1 survey scans were acquired from *m*/*z* 300 to 1,500 at a resolution of 120,000 using the Orbitrap mode. The most intense ions were isolated for 3 seconds with a 1.2 *m*/*z* window and then fragmented by high-energy collision-induced dissociation (HCD) with a normalized collision energy of 35%, considering a dynamic exclusion of 30 seconds. MS/MS spectra were recorded using normal speed IonTrap mode.

Data evaluation was performed with PEAKS ONLINE software using 15 ppm for precursor mass tolerance, 0.5 Da for fragment mass tolerance, specific tryptic digest and a maximum of 3 missed cleavages. NBF (+163.00961594 Da) on C, K and R, and DCP (+168.0786442 Da) on C were added as variable modification, peptide-spectrum match (PSM), and proteins were filtered at FDR 1%.

Total proteome analysis

Protein digestion and peptide fractionation. 100ug of the NBF-Cl labeled samples were saved for whole proteome analysis. Samples were precipitated using methanol/chloroform precipitation to remove all detergent. Pellets were resuspended in digestion buffer supplemented with 0.1 M urea (Sigma, U5378) and digested at 1:20 trypsin:protein ratio overnight. Peptides were then desalted as previously described and evaporated to dryness.

Before the fractionation peptides were resuspended in 0.1% TFA and the peptide concentration was determined using amino acid analysis according to Cohen et al. Quantification was conducted against an eight-point calibration curve of derivatized amino acids in the range from (1-50 pmol/µL) using a Vanquish Flex UHPLC (Thermo Fisher, Bremen, Germany) for separation. For the Fractionation, the Pierce™ High pH Reversed-Phase Peptide Fractionation Kit (Thermo Fisher Scientific, 84868) was used. 40 µg of each sample were fractionated following the manufacturer instruction. Shortly, peptides were loaded onto the columns then eluted with different percentages of acetonitrile into 8 fractions. All fractionated samples were then evaporated to dryness and resuspended in 0.1% TFA before being analyzed by LC-MS.

LC-MS/MS and data analysis (total proteome). Samples were analyzed by LC-MS using the same instruments described in the aboved “persulfide-specific proteomics“ section.

A different 90 min HPLC gradient was programmed for each fraction (**Fraction 1**: 0 min, 3% B; 75min, 20% B; 95 min, 35% B | **F2**: 0 min, 3% B; 88min, 29% B; 95 min, 35% B | **F3**: 0 min, 3% B; 92min, 31% B; 95 min, 35% B | **F4**: 0 min, 3% B; 12 min, 7% B; 92min, 32% B; 95 min, 35% B| **F5**: 0 min, 3% B; 12 min, 8% B; 92min, 32% B; 95 min, 35% B | **F6**: 0 min, 3% B; 12 min, 8% B; 92min, 33% B; 95 min, 35% B | **F7**: 0 min, 3% B; 12 min, 8% B; 95 min, 35% B | **F8**: 0 min, 3% B; 10 min, 8% B; 95 min, 42% B). The same parameters as previously described were used for MS analysis as well as for the PEAKS online search parameters. Only the DCP modification has been removed.

Determination of the ZF Proteome in MEF Cells. The ZFs that were detected by direct proteomics in MEF cells were obtained by comparing the list of proteins obtained from the proteomics data with the ZF proteins that have been annotated in the UniProt database (“zinc finger protein”) from the organism “mouse”. The reviewed ZF protein list that was utilized is number: UP0000000589 and it contains 1391 ZF. For each identified protein, the ZF classification was retrieved from Uniprot. Each ZF was then grouped manually based upon the cysteine and histidine content of the zinc finger domains. Four main classification types were applied: CCCC, CCCH, CCHC and CCHH, with C = cysteine and H = histidine. The number of ZFs with 4 cysteines, 3 cysteines or 2 cysteines were then determined. This involved grouping the ZF proteins that were annotated as CCCH with those annotated as CCHC. If a protein had more than one type of ZF present in its domain, both types were counted. All ZFs sorted have confirmed “Zinc Finger Protein” annotations on Uniprot. Putative ZF-containing proteins are not used in this study.

Identification of persulfidated ZFs in MEF cells. The ZF proteins that were detected in cells to which the persulfide specific proteomic approach was applied were identified in the same manner as the ZFs identified for the direct proteomics approach, using Uniprot (*vide supra*).

Identification of persulfidated ZFs in A431, A549, U2OS, HEK293, MDA-MB-231 cells. The ZF proteins present in published persulfide specific proteomics data in human cells (A431, A549, U2OS, HEK293, MDA-MB-231)[15] were obtained in the same manner as for our experimental data, using UniProt, except that the ZFs identified in ‘human’ was utilized as the UniProt list. This reviewed list, # UP0000005640 contains 1912 proteins. The ZFs that

were identified were then sorted following the same method as for MEF cells. For detailed experimental methods and sorting of proteomics, ZFs, and persulfidated ZFs, refer to Table S1 and S2.

Purification of TTP peptides: TTP-D2 (CCCH), TTP-D1 (CCCH), TTP-D1 (CCCC), TTP-D1 (CCHH), and TTP-D1 (CHHH). Further purification of purchased peptides was achieved via a Waters HPLC with a Waters Symmetry C-18 preparative column using a CH_3CN/H_2O gradient both containing 0.1% TFA. TTP peptides were first incubated with 15 mM TCEP for 15 mins while mixing before being injected. Elution of a single, defined peak at ~ 67% H_2O (0.1% TFA) afforded the isolated peptides, which were lyophilized to dryness in an anaerobic chamber (3% H_2/97% N_2) using a Thermo SPD speedvac and stored at -80°C until use. Purity was estimated to be >95% pure on the basis of the HPLC chromatogram and MALDI identification of the expected $(m/z)^+$ within $\pm$ 0.1 $(m/z)^+$.

A two-domain construct of TTP (TTP-2D), containing both CCCH zinc finger domains was over-expressed and purified as previously reported.[11a, 18]

TTP peptide sample preparation, anaerobic measurements, and statistical analysis. Peptide manipulations and UV-visible titrations were performed in a Coy anaerobic chamber (3% H_2 / 97% N_2) unless otherwise specified. UV-visible spectroscopy was performed in 1 cm pathlength quartz cuvettes (Starna Cells) using a Cary 60 UV-Vis Spectrophotometer (Agilent). For circular dichroism (CD), samples were prepared in the anaerobic chamber with 1 mm quartz and 5 mm Spectrosil quartz cuvettes (Starna Cells), respectively, and Teflon-stoppered for measurements outside the Coy anaerobic chamber. All analyses were performed in triplicate. Statistical variation in binding affinities, fold change, and normalized fluorescence were calculated as standard error of the mean (SEM).

Metal binding titrations of TTP peptides. Metal binding titrations for TTP-D2, TTP-D1-CCCH, -CCCC, -CCHH, and -CHHH peptides were performed anaerobically. For each titration, $CoCl_2$ was added to apo-peptide in increments of 0.1 molar equivalents up to 1 equivalent, followed by 1-equivalent additions up to 10 equivalents. During the titration, d-d transition bands from 500 to 700 nm (maxima vary per peptide/ligand set) for Co^{II}-peptide binding were observed. The data were fit to a 1:1 binding model and an upper limit K_d was determined. $Zn(OAc)_2$ was then added to the Co^{II}-bound sample in the same increments. The d-d transitions between 500-700 nm decreased. These data were fit using a competitive binding model to determine an upper limit dissociation constant (K_d) for Zn^{II}.[18]

$$\text{Co-TTP} + Zn^{II} \rightleftharpoons \text{Zn-TTP} + Co^{II}$$

Intrinsic tyrosine fluorescence of TTP peptides. Tyrosine fluorescence (3 Tyr residues per peptide) for TTP-D2, TTP-D1-CCCH, -CCCC, -CCHH, and -CHHH peptides was measured in 50 mM sodium phosphate buffer, pH 7.5, using 1 cm pathlength cuvettes (Firefly Sci) and a K2 spectrofluorimeter (ISS, Inc.). Excitation spectra for each peptide were collected from 200 to 290 nm to determine the maximal excitation wavelength for emission at 303 nm. Both the excitation and emission slit widths were set to 1 mm. An excitation wavelength of 230 nm was used to observe emission from 290 to 360 nm, with a λ_{Max} of 303 nm. Scans were collected of both the apo-peptide (5 µM) and following a 1-equivalent addition of Zn^{II}. The $Intensity_{Max}$ was compared between apo- and Zn-bound TTP and related as follows:

$$\text{Fold increase} = \text{Intensity}_{Max}\ (\text{apo-TTP}) / \text{Intensity}_{Max}\ (\text{Zn-TTP})$$

Zn-TTP-D1-CCCH and -D2-CCCH were separately treated with Na_2S (10 eq) and the emission at 303 nm was collected every 5 minutes, up to 30 minutes.

Circular dichroism (CD) of TTP peptides. Circular dichroism spectra were measured for the TTP-D2, TTP-D1-CCCH, -CCCC, -CCHH, and -CHHH peptides from 190 to 250 nm using a Jasco-1500 spectropolarimeter. Peptides were prepared at 25 µM in 20 mM sodium phosphate buffer, pH 7.5. Apo-peptide was first scanned followed by a scan with 1-eq of zinc(II), with both corrected for the initial spectrum obtained of buffer alone. The scanning speed was 100 nm/min, with 1 mm bandwidth, for a total of 3 scans that were averaged for the final plot.

Preparation of H_2S. Na_2S powder was aliquoted into screw-capped amber vials that were wrapped in parafilm and stored in a Coy anaerobic chamber (3% H_2 / 97% N_2). Degassed Milli-Q water was applied to Na_2S to generate fresh H_2S stock solutions daily for use in experiments. Stock solutions of HS^- were quantified by UV-visible absorption at 230 nm (ε = 7800 M^{-1} cm^{-1}) and further dilutions were made.

Cryo-electrospray-ionization mass-spectrometry (CSIMS) of TTP-1D Peptides. Zn-TTP peptides (40 µM) in 20 mM ammonium bicarbonate buffer were mixed with Na_2S solution (1:10, mole/mole) under aerobic condition

and immediately connected to mass spectrometer. Mass spectrometric measurements were performed on a UHR-TOF MS (ultra high resolution time of flight mass spectrometer) maXis 4G (Bruker Daltonik, Bremen, Germany) coupled to a Bruker cryospray unit. The resolution of the ESI-TOF MS is at least 40 000 full-width at half maximum. Detection was in the positive-ion mode. The flow rates were 500 µL/h. The drying gas (N_2), was held at 10 °C and the spray gas (N_2) was held at 5 °C. The instrument was calibrated prior to each experiment via direct infusion of the Agilent ESI-TOF low concentration tuning mixture, which provided an m/z range of singly charged peaks up to 2700 Da in both ion modes. Spectra were processed using Data Analysis software (Bruker Daltonik, Bremen, Germany).

Dimedone switch labeling of TTP-2D and -1D Peptides during reaction with H_2S. 15 µM Zn-TTP-X (X= 2D, D2-CCCH, D1-CCCH, D1-CCCC, D1-CCHH, and D1-CHHH) solution was prepared by mixing apo-TTP with $ZnCl_2$ (30 µM for TTP-2D and 15 µM for TTP-1D peptides) in a quartz cuvette under anaerobic conditions. Initial UV-visible spectra were obtained for the apo-TTP and following Zn(II) addition. Na_2S in H_2O was then added for a final concentration of 15 µM. The cuvette was removed from the glove box, opened to air, mixed vigorously, and placed back in the glove box. NBF-Cl was then added for a final concentration of 100 µM and the UV-visible spectrum from 220 and 820 nm was recorded. The UV-visible spectrum was then recorded every 30 seconds until no changes between the 400-500 nm region were observed (typically 10-20 minutes). At this point, dimedone was added for a final concentration of 200 µM and the UV-visible spectrum of the sample recorded, at t=0 and subsequently every 30 seconds until no further decrease in the absorbance between the 420-430 nm region was observed.

Hydroethidine to measure superoxide via spectrofluorimetry during reactions of TTP peptides with H_2S. Zn-TTP-D2-CCCH, -TTP-D1-CCCH, -CCCC, -CCHH, and -CHHH were prepared at 20 µM in 50 mM sodium phosphate buffer, pH 7.5. The fluorescence emission spectra of each Zn-peptide were measured on an ISS K2 spectrofluorimeter using an excitation of 466 nm and measuring the emission between 510 to 680 nm with slit widths set to 0.5 and 2 mm, respectively. These parameters were based upon a xanthine/xanthine oxidase (XOD) control (100 µM HE, 1 mM xanthine, 50 mU/mL xanthine oxidase in 100 mM potassium phosphate buffer, pH 7.5) for which a superoxide radical and the hydroethidine oxidation product specific to that oxidant, 2-OH-E^+ was generated and measured.[22] The experimental conditions were 1) Zn-TTP-1D alone, 2) Zn-TTP-1D + 150 µM HE, and 3) Zn-TTP-1D + 150 µM HE + 2 mM Na_2S. Buffer was O_2-sparged just prior to preparing condition 1, which was then assessed by intrinsic Tyr fluorescence (excitation: 230 nm, max emission: 303 nm) to ensure consistent fluorescence intensities across samples, confirming peptide fold/Tyr environment prior to starting. Emission spectra for conditions 2 and 3 were then measured at 15, 30, 45, 60, 90, and 120 minutes, with excitation spectra collected again after 120 minutes. Samples were stirred with a stir bar and left uncapped during the reaction. Samples were also visually observed after 120 minutes and the following day for the color exhibited by the oxidation products of hydroethidine. To assess ROS production via HE oxidation between the Zn-TTP-1D peptides, condition 2 was used to correct the average fluorescence endpoint (at 2 hours) for condition 3 as follows:

corrected fluorescence = average sample intensity – control intensity.

Synthetic procedures. All syntheses and manipulations were conducted in an N_2-filled drybox (Vacuum Atmospheres, O_2 < 0.2 ppm, H_2O < 0.5 ppm) or using standard Schlenk techniques under an atmosphere of Ar unless otherwise noted.

Instrumentation. The ^{1}H NMR spectra were measured on a Bruker 400 MHz spectrometer. Chemical shifts were referenced to the reported solvent resonances. High resolution EI mass spectra were obtained using a VG70S double-focusing magnetic sector mass spectrometer (VG Analytical, Manchester, UK, now Micromass/Waters) equipped with an MSS data acquisition system (MasCom, Bremen, Germany). Negative mode electrospray ionization mass spectra (ESI-MS) were collected on a Waters SYNAPT G2S HDMS Q-TOF Mass Spectrometer. Attenuated total reflectance (ATR) infrared spectra were obtained with a Golden Gate Reflectance diamond cell in a Nexus 670 Thermo-Nicolet FTIR spectrometer.

Synthesis of $[(PPh_3)_2N][SH]$. The preparation of $[(PPh_3)_2N][SH]$ was modified from a previously published synthesis (48). An amount of $[(PPh_3)_2N]Cl$ (1.15 g, 2.0 mmol) was dissolved in CH_3CN (8 mL). The solution was added dropwise to anhydrous NaSH (0.15 g, 2.6 mmol), forming a lime green solution with a white solid. The mixture was stirred at 23 ºC for 3 days and the resulting light-yellow solution was filtered, and the filtrate was dried under vacuum. The resulting solid was washed with Et_2O and dried to give an off white, glassy solid (1.09 g, 95%). ^{1}H NMR (CD_3CN, 400 MHz): δ = 7.71-7.48 (m, 30H, Ar), -3.94 (s, br, 1H, S*H*) ppm.

Synthesis of Zn(PATH)(SH). A solution of $[(PPh_3)_2N][SH]$ (60 mg, 0.11 mmol) in CH_3CN (1.5 mL) was added to a solution of Zn(PATH)Br (40 mg, 0.11 mmol) in CH_3CN (3 mL) to afford a white suspension. The reaction mixture

was stirred for 30 min at 23 ºC, and then filtered through Celite. The filtrate was left to stand at -30 ºC, resulting in the formation of colorless crystals (blocks, 10 mg (31%)) suitable for X-ray structure determination after 2 days. ^{1}H-NMR (CD_3CN, 400 MHz): δ = 8.71 (d, J = 5.2 Hz, 1H, py-H_α), 7.97 (td, J = 1.7, 7.7 Hz, 1H, py-H_γ), 7.52 (m, 1H, py-H_δ), 7.46 (d, J = 7.9 Hz, 1H, py-$H_ß$), 3.45-3.29 (m, 1H, CH_2), 3.10-2.80 (m, 4H, CH_2CH_2), 2.70 (s, 3H, N-CH_3), 2.52 (d, J = 13.2 Hz, 1H, CH_2), 1.47 (s, 3H, CH_3), 1.25 (s, 3H, CH_3), -1.94 (s, 1H, S*H*) ppm.

Generation of $[Zn(PATH)(SH)_2]^-$. The bis(hydrosulfide) complex $[Zn(PATH)(SH)_2]^-$ (**3**) can be generated in situ starting from either Zn(PATH)Br (**1**), or from isolated, crystalline Zn(PATH)(SH) (**2**). In a typical procedure, a stock solution of $[(PPh_3)_2N][SH]$ (36 mg, 0.06 mmol) in CD_3CN (1.5 mL) was added in 50 µL portions (3 equiv) to a solution of Zn(PATH)Br (4 mg, 0.01 mmol) in CD_3CN (350 µL). The solution turned cloudy after the addition of 1 equiv of $[(PPh_3)_2N][SH]$, and then turned clear following the addition of more $[(PPh_3)_2N]SH$. Analysis by ^{1}H-NMR spectroscopy confirmed the formation of complex **3,** which is stable in solution for at least 16 hours. ^{1}H NMR (CD_3CN, 400 MHz): δ = 8.49 (d, J= 3.8 Hz, 1H, py-H_α), 7.51 (d, J= 7.9 Hz, 1H, py-H_δ), 7.27 (m, 1H, py-$H_ß$), 3.26 (m, 4H, CH_2CH_2), 2.70 (s, 3H, N-CH_3), 2.58 (m, 2H, CH_2), 1.48 (s, 6H, CH_3) ppm. HRMS (ESI) m/z: *calcd* for $[M]^-$ = 353.0158, observed mass: 353.0112.

Persulfidation reaction of $[Zn(PATH)(SH)_2]^-$ (3) with O_2. A solution of $[(PPh_3)_2N][SH]$ (180 mg, 0.31 mmol) in CH_3CN (5 mL) was added dropwise to crystalline Zn(PATH)Br (40 mg, 0.11 mmol) dissolved in CH_3CN (3 mL), generating $[Zn(PATH)(SH)_2]^-$ in situ over the course of 10 minutes. Excess O_2 was added by bubbling for 5 minutes, causing the slightly cloudy, colorless solution to turn light yellow. The reaction mixture was left to stir for 3 hours, over which time the solution turned a darker yellow. A solution of 6 M HCl (5 mL) was added, and the resulting clear lime green solution was left to stir for 30 minutes. The solution was then diluted with DI water (10 mL) and washed with CH_2Cl_2 (4 x 7 mL). The aqueous layer was neutralized with the dropwise addition of concentrated NH_4OH, and subsequently extracted with diethyl ether (4 x 5 mL). The organic layer was concentrated in vacuo to yield a mixture of PATH and persulfidated PATH (2-methyl-1-[methyl(2-pyridin-2-ylethyl)amino]propane-2-perthiol) as a light-yellow oil (*caution*: the crude product has a strong, noxious smell related to H_2S and should be handled in a well-ventilated hood or other lab space). The yield of the persulfidated product was determined by integration of ^{1}H-NMR spectra and comparison with peaks from 1,3,5-trimethoxybenzene added as an internal standard (yield: 11.8% ± 0.2 %, (average of 3 runs)). Characterization data for persulfidated PATH: ^{1}H-NMR: ($CDCl_3$, 400 MHz): δ = 8.49 (m, 1H, py-H_α), 7.58 (m,1H, py-H_γ), 7.18 (t, J= 7.2 Hz, 1H, py-H_δ), 7.08 (m, 1H, py-$H_ß$), 2.88 (m, 4H, CH_2CH_2), 2.59 (s, 2H, CH_2), 2.42 (s, 3H, N-CH_3), 1.27 (s, 6H, CH_3) ppm. (CD_3CN, 400 MHz): δ = 8.48 (m, 1H, py-H_α), 7.65 (m,1H, py-H_γ), 7.25 (t, J= 7.2 Hz, 1H, py-H_δ), 7.15 (m, 1H, py-$H_ß$), 2.89 (m, 4H, CH_2CH_2), 2.59 (s, 2H, CH_2), 2.41 (s, 3H, N-CH_3), 1.26 (s, 6H, CH_3) ppm. HRMS (EI) m/z: *calcd* for $[M]^+$= 256.1067, observed mass: 256.1071.

Single crystal x-ray crystallography. All reflection intensities were measured at 110(2) K using a SuperNova diffractometer (equipped with Atlas detector) with Mo *K*α radiation (λ = 0.71073 Å) under the program CrysAlisPro (Version CrysAlisPro 1.171.39.29c, Rigaku OD, 2017). The same program was used to refine the cell dimensions and for data reduction. The structure was solved with the program SHELXS-2018/3 and was refined on F^2 with SHELXL-2018/3. [1] Numerical absorption correction based on gaussian integration over a multifaceted crystal model was applied using CrysAlisPro. The temperature of the data collection was controlled using the system Cryojet (manufactured by Oxford Instruments). The H atoms were placed at calculated positions (unless otherwise specified) using the instructions AFIX 23, AFIX 43 or AFIX 137 with isotropic displacement parameters having values 1.2 or 1.5 U_{eq} of the attached C atoms. The H atom attached to S2 (thiolate) was found from a difference Fourier map, and its coordinates were refined freely. The occupancy factor of S2 was initially refined freely to check for possible impurities (Br), and the occupancy factor refined to 0.995(2), which strongly suggests S2 is fully occupied. In the final refinement, its occupancy factor was constrained to 1.

Results and Discussion

Table S1. Total proteome (n=5927) and total persulfidome (n=2435) identified from MEF cells.

This file contains two sheets: one for the list of proteins identified in total proteomics and one for the list of proteins identified in the persulfide-enriched dimedone switch proteomics. All mass spectrometric proteomics data, protein identification, and quantification results have been deposited with the ProteomeXchange Consortium via the PRIDE partner repository with the dataset identifier PXD041310 and 10.6019/PXD041310.

Table S2. Total ZFs (n=471) and total persulfidated ZFs (n=118) from MEF and additional cell lines.

This file contains only the full list of persulfidated ZFs in MEF cells, as well as the matching ZFs found in the persulfide-specific proteomics from the additional 5 cell lines from Fu et al.

Table S3. Amino acid sequence alignments of the TTP-1D peptides. Zn^{II} ligands are highlighted in purple and Tyr, used for intrinsic fluorescence studies, in green.

A	N	R	H	P	K	Y	K	T	E	L	C	H	K	F	Y	L	Q	G	R	C	P	Y	G	S	R	C	H	F	I	H	N	P	T	E	D	[a]
D1 CCCH		T	S	S	R	Y	K	T	E	L	C	R	T	Y	S	E	S	G	R	C	R	Y	G	A	K	C	Q	F	A	H	G	L	G	E	L	R	Q
D1 CCCC		T	S	S	R	Y	K	T	E	L	C	R	T	Y	S	E	S	G	R	C	R	Y	G	A	K	C	Q	F	A	C	G	L	G	E	L	R	Q
D1 CCHH		T	S	S	R	Y	K	T	E	L	C	R	T	Y	S	E	S	G	R	C	R	Y	G	A	K	H	Q	F	A	H	G	L	G	E	L	R	Q
D1 CHHH		T	S	S	R	Y	K	T	E	L	C	R	T	Y	S	E	S	G	R	H	R	Y	G	A	K	H	Q	F	A	H	G	L	G	E	L	R	Q

[a] Sequence for TTP-D2

Table S4. Upper limit binding affinities (K_d's) for Co^{2+} for the TTP variants. Experiments were performed in 100 mM HEPES, pH 7.5. Numbers following the ± are calculated SEM from replicate experiments (N=3).

TTP Peptide	Co^{II} K_d (M)
D2-CCCH	$3.9 \times 10^{-7} \pm 3.8 \times 10^{-8}$
D1-CCCH	$4.0 \times 10^{-7} \pm 7.1 \times 10^{-8}$
D1-CCCC	$1.4 \times 10^{-6} \pm 1.5 \times 10^{-7}$
D1-CCHH	$4.2 \times 10^{-6} \pm 1.1 \times 10^{-6}$
D1-CHHH	$5.0 \times 10^{-4} \pm 2.4 \times 10^{-5}$

Table S5. Relative hydroethidine fluorescence for the ZF peptides. Corrected fluorescence of HE oxidation for the ZF peptides (Average sample – Control sample of TTP-1D peptide + HE without Na_2S) and their normalization to the maximal peptide, D1-CCCH. Numbers following the ± are calculated SEM from replicate experiments (N=3).

TTP Peptide	Corrected Fluorescence [a]	Normalized to TTP-D1-CCCH
D1-CCCH	244111	1.00 ± 0.03
D2-CCCH	200009	0.82 ± 0.05
D1-CCCC	100971	0.41 ± 0.02
D1-CCHH	120247	0.49 ± 0.02
D1-CHHH	98268	0.40 ± 0.04

[a] Respective TTP + HE without Na_2S

Table S6. Experimental details for the XRD data for compound **2**

	2
Crystal data	
Chemical formula	$C_{12}H_{20}N_2S_2Zn$
M_r	321.79
Crystal system, space group	Monoclinic, $P2_1/n$
Temperature (K)	110
a, b, c (Å)	8.1788 (2), 14.9782 (4), 11.8161 (3)
β (°)	92.434 (2)
V (Å^3)	1446.21 (6)
Z	4
Radiation type	Mo $K\alpha$
μ (mm^{-1})	1.97
Crystal size (mm)	0.35 × 0.21 × 0.16
Data collection	
Diffractometer	SuperNova, Dual, Cu at zero, Atlas
Absorption correction	Gaussian *CrysAlis PRO* 1.171.41.93a (Rigaku Oxford Diffraction, 2020) Numerical absorption correction based on gaussian integration over a multifaceted crystal model Empirical absorption correction using spherical harmonics, implemented in SCALE3 ABSPACK scaling algorithm.
T_{min}, T_{max}	0.433, 1.000
No. of measured, independent and observed [$I > 2\sigma(I)$] reflections	17010, 3328, 3034
R_{int}	0.032
$(\sin\theta/\lambda)_{max}$ (Å^{-1})	0.650
Refinement	
$R[F^2 > 2\sigma(F^2)]$, $wR(F^2)$, S	0.023, 0.055, 1.02
No. of reflections	3328
No. of parameters	160
H-atom treatment	H atoms treated by a mixture of independent and constrained refinement
$\Delta\rho_{max}$, $\Delta\rho_{min}$ (e Å^{-3})	0.37, -0.41

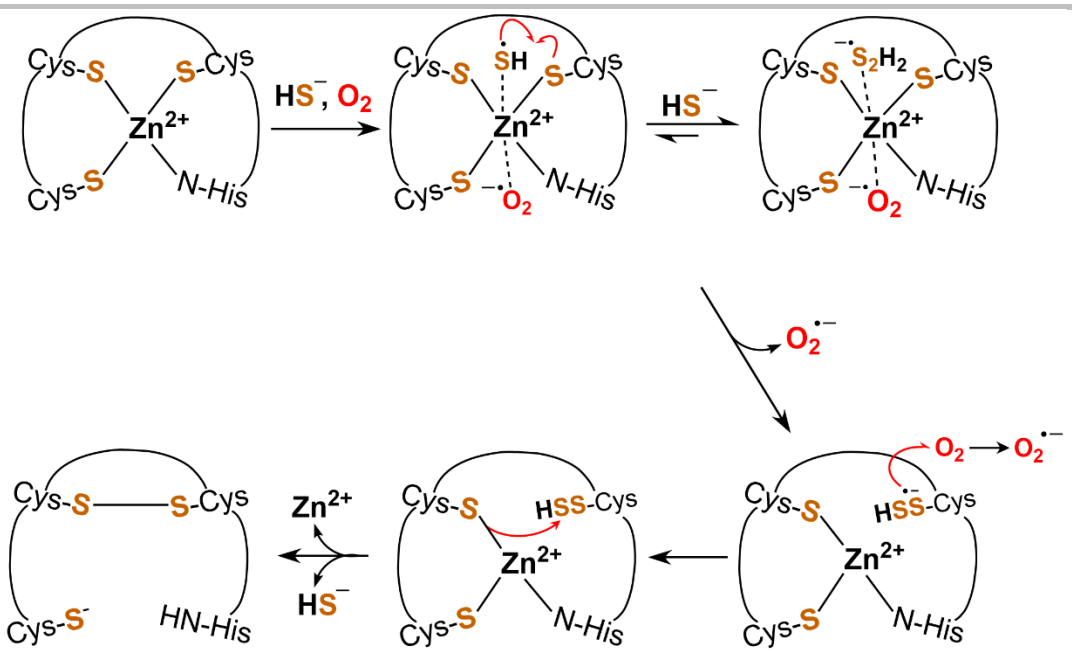

Scheme S1. Proposed mechanism for the persulfidation of zinc finger domains by H_2S in the presence of O_2. The initial HS^- coordination to the Zn^{II} site, which acts as a conduit for the anionic species present, facilities reduction of O_2 and activation of HS^- to the thiyl radical species ($HS^{\bullet}$). This species could react with additional HS^- present or form a perthiyl radical ($HSS^{\bullet -}$) with a proximal Cys residue. Further reaction with ambient oxygen can form the persulfide group (SSH), and depending upon the current oxidative environment, the complete oxidation to a disulfide bond occurs.

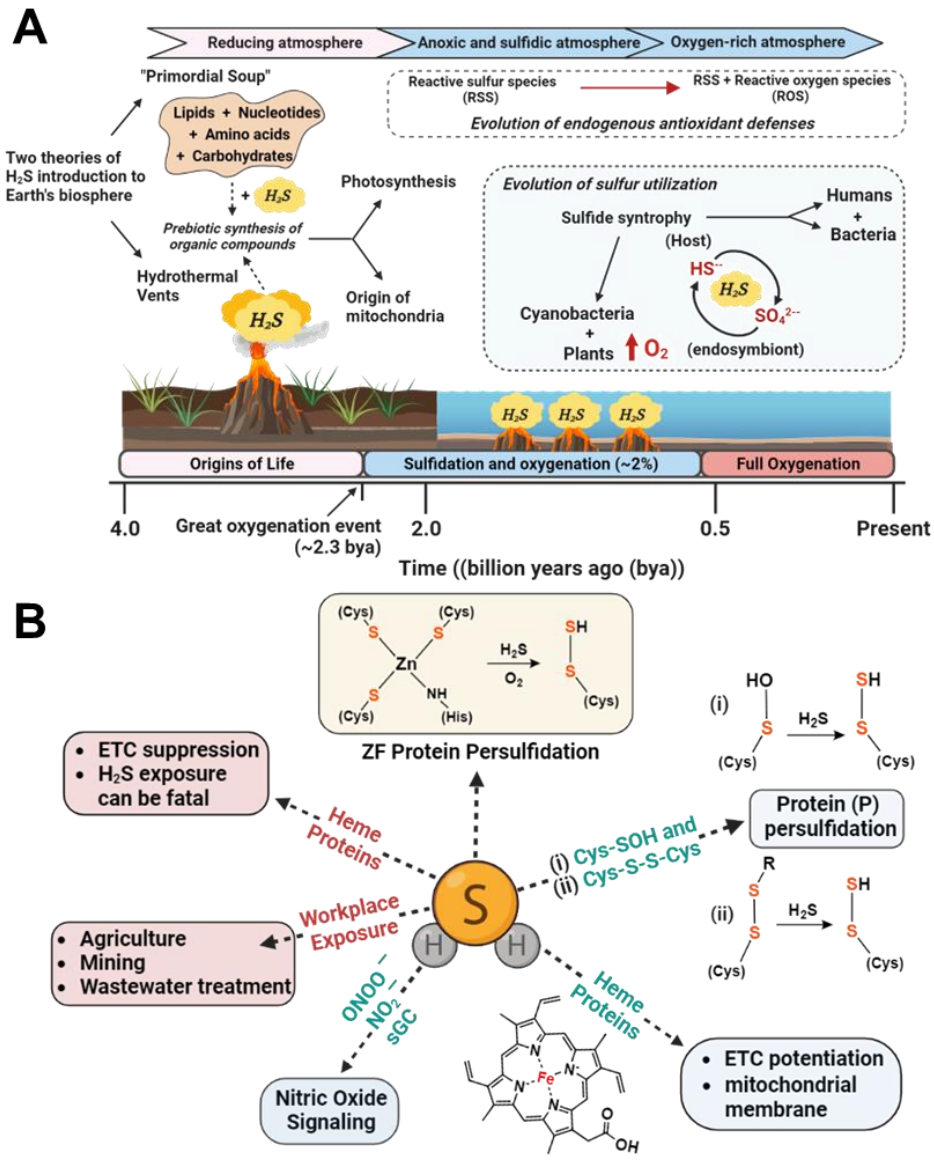

Figure S1. The role of hydrogen sulfide (H_2S) throughout evolution and known effects in mammalian biology. A) The geological abundance of H_2S and its utility to the evolution of early life in an oxygen-restricted atmosphere.[2] **B)** Examples of the chemical biology of H_2S/HS^-. Endogenously produced H_2S in mammals is involved in crosstalk with nitric oxide (NO) signaling (examples: peroxynitrite ($ONOO^-$), nitrite (NO_2^-), and soluble guanylate cyclase (sGC)), serves as a reducing source for the electron transport chain (ETC) and mitochondrial membrane energetics, and signals by direct (and indirect) persulfidation of Cys residues.[1]

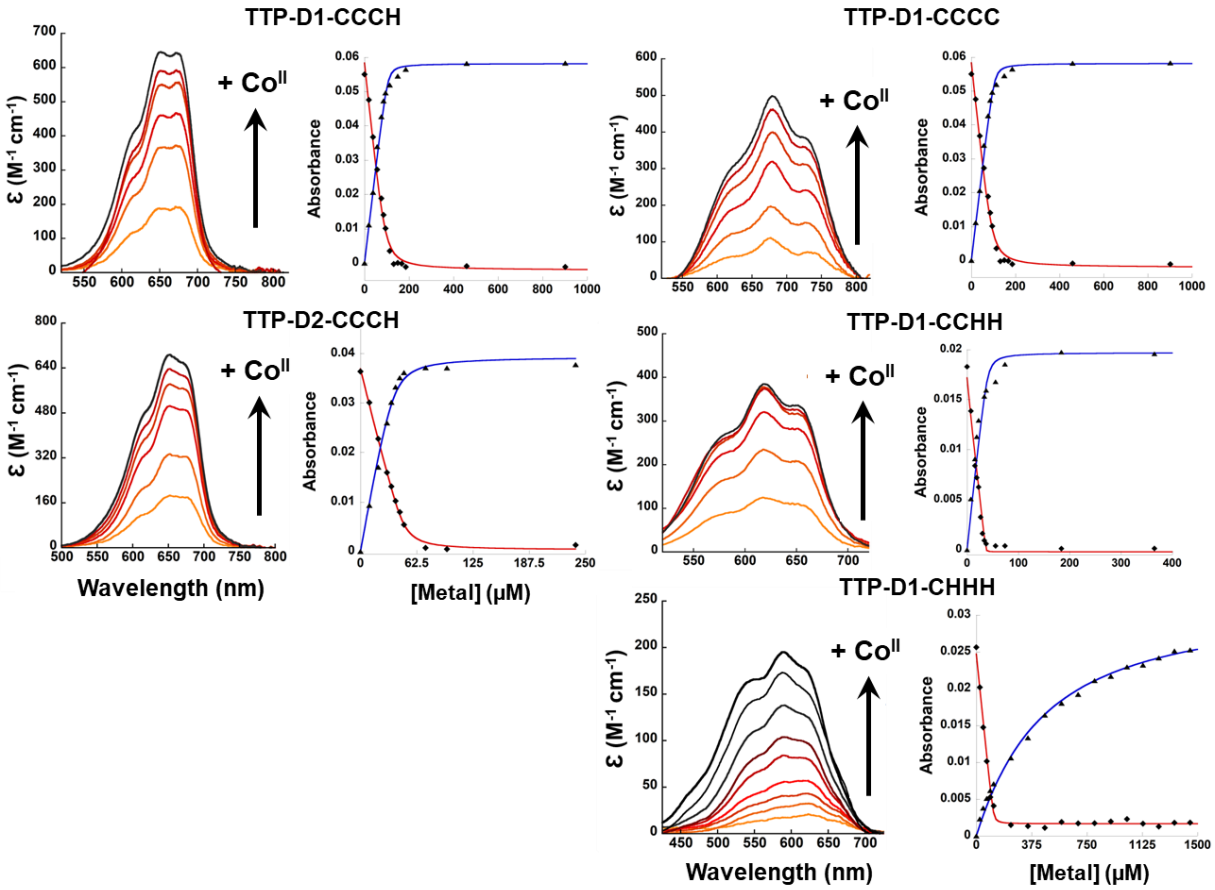

Figure S2. Absorption spectra of the Co(II) d-d transition bands during titration of apo-TTP-1D variants with $CoCl_2$. *Left:* plots of the change in the absorption spectrum as apo-TTP-1D variants are titrated with $CoCl_2$. *Right:* plots of the change in the absorbance spectra at 680 nm for TTP-D1-CCCC, 650 nm for TTP-D1- and D2-CCCH, 620 nm for TTP-D1-CCHH, and 580 nm for TTP-D1-CHHH as a function of Co^{2+} (blue) and Zn^{2+} (red) concentration. The solid lines (blue: Co^{2+}, red: Zn^{2+}) are fit to 1:1 and competitive binding equilibria (K_d's), respectively. Experiments were performed in 100 mM HEPES, pH 7.5.

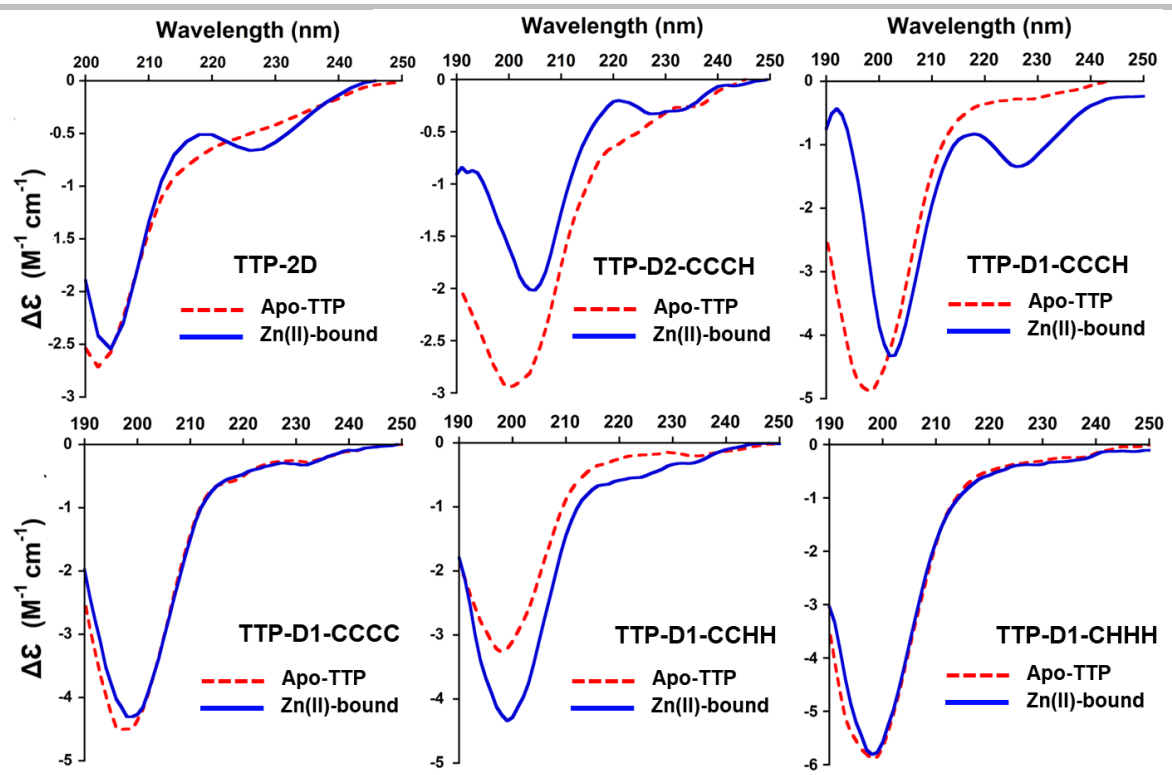

Figure S3. Circular Dichroism (CD) spectra for TTP variants in the apo- and Zn^{II}-bound states. CD spectra between 190 and 250 nm for the TTP ZF peptide variants before and after Zn^{II} addition. All experiments were performed in 20 mM sodium phosphate buffer, pH 7.5.

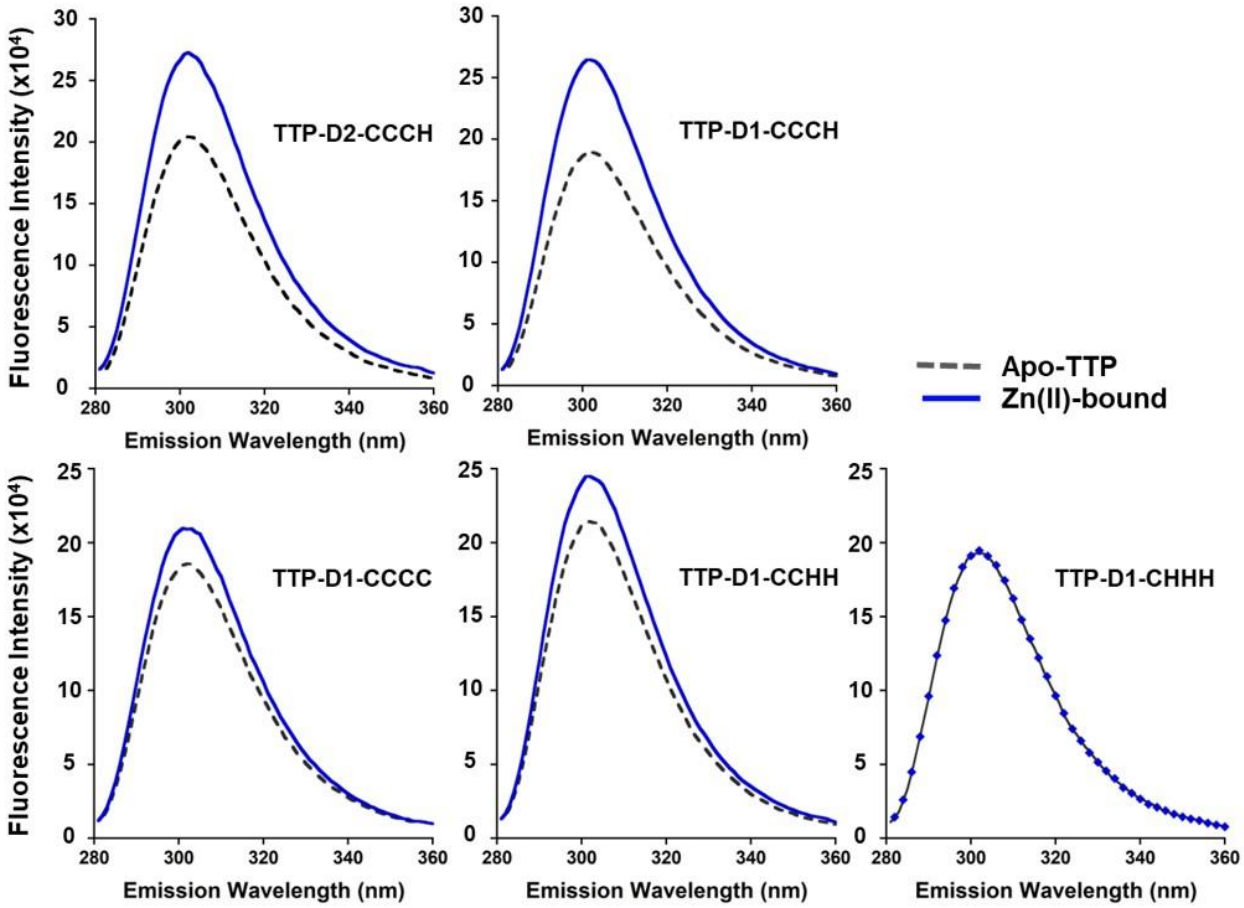

Figure S4. Intrinsic tyrosine fluorescence of TTP peptides in apo- and Zn^{II}-bound forms. Fluorescence emission of Tyr (λ_{ex} = 230 nm) from 280 to 360 nm for the TTP peptide variants before and after Zn^{II} addition. All experiments were performed in 50 mM sodium phosphate buffer, pH 7.5.

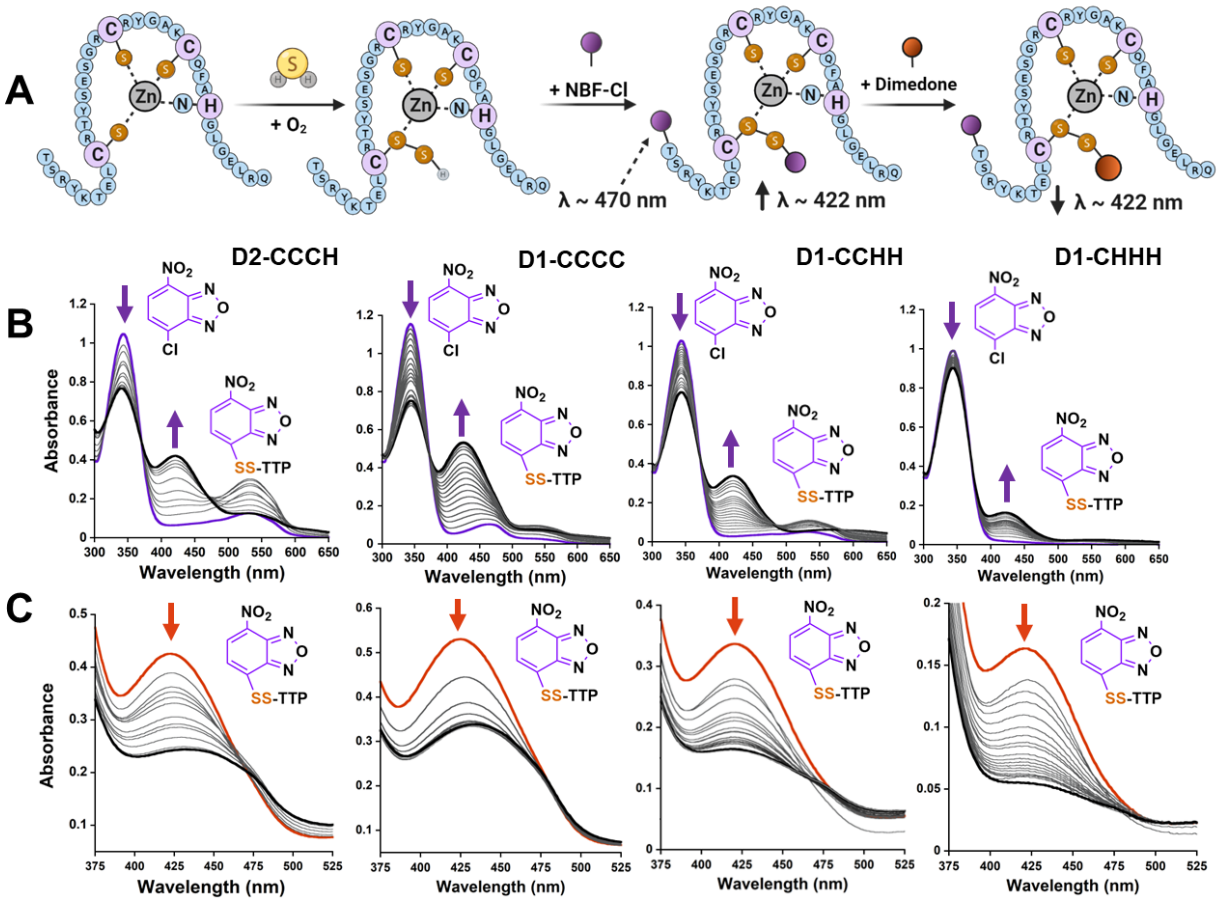

Figure S5. Detection of protein persulfides formed *in situ* by reaction of Zn-TTP-1D peptides and H_2S. A) Reaction scheme for the dimedone switch in-solution method for detection of TTP-persulfides using UV-visible spectroscopy. **B)** UV-Visible spectra of Zn-TTP peptides reacted with Na_2S after exposure to O_2 and addition of NBF-Cl (purple), scanned every 30s (grey traces) until no further change was observed (black). **C)** Plot of spectra immediately following addition of dimedone to the same reaction mixture (red), scanned every 30s (grey traces) until no further change was observed (black). The reaction conditions were 15 µM Zn-TTP peptide (pre-incubated with 15 µM $ZnCl_2$), 15 µM Na_2S, 100 µM NBF, 200 µM dimedone, in 100 mM HEPES buffer, pH 7.5.

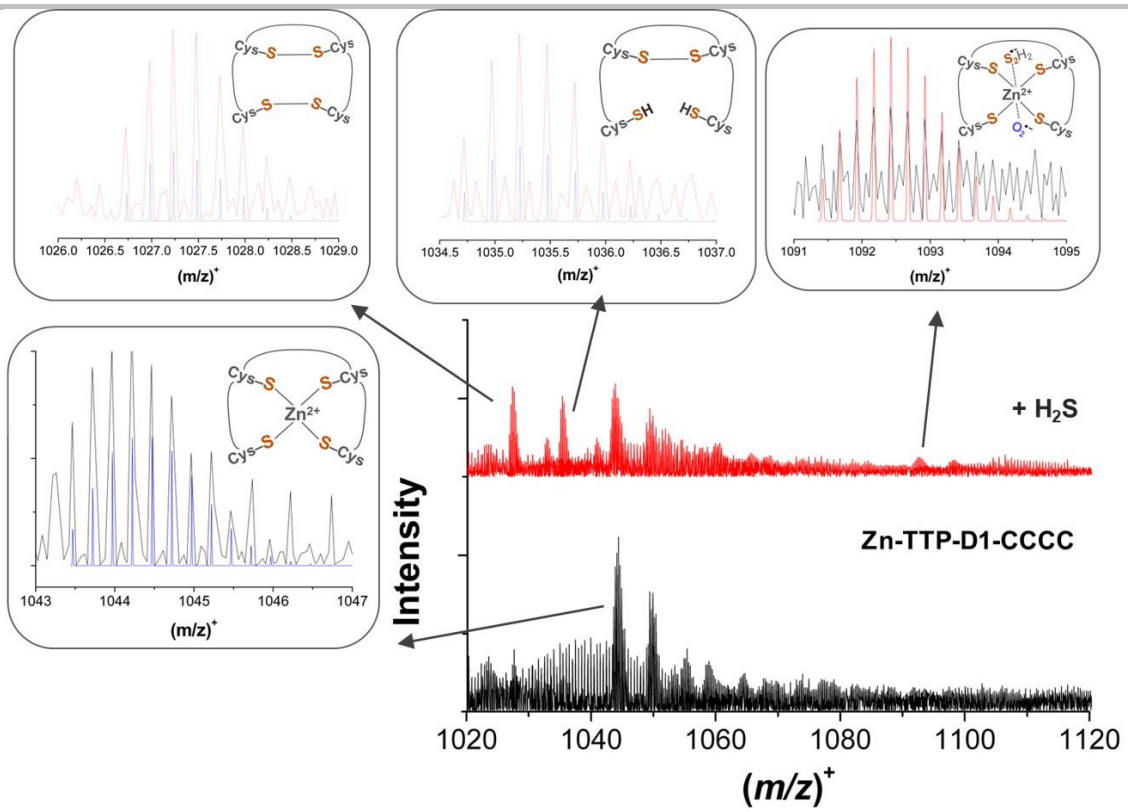

Figure S6. CSI-MS of TTP-D1-CCCC peptide reacted with H_2S. CSI-MS spectra of the z = 4+ species of Zn-TTP-D1-CCCC peptide before (black spectrum) and after (red spectrum) aerobic reaction with H_2S. Experimental and simulated adducts are overlaid for unreacted peptide (black and blue, respectively) and for peptide reacted with H_2S (blue and red, respectively); top right: $[Zn\text{-}TTP\text{-}D1\text{-}CCCC + O_2^{\bullet-} + H_2S_2^{\bullet-}]^{4+}$

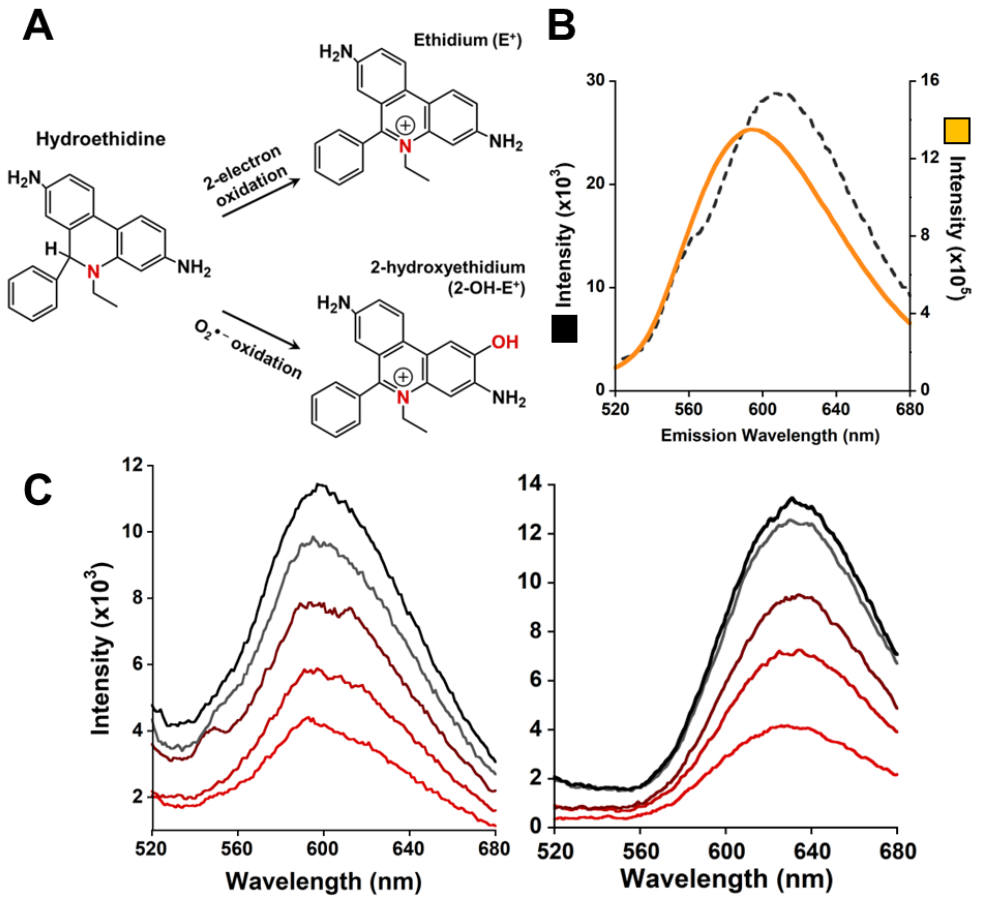

Figure S7. Control experiments for hydroethidine (HE) fluorescence increase from oxidative species. A) Chemical structures of HE and two of its oxidation products. **B)** Xanthine/xanthine oxidase (XOD) control demonstrating initial, red-shifted fluorescence signal (black, λ_{max} ~ 610 nm) and following 30 minutes, blue-shifted fluorescence signal (orange, λ_{max} ~595 nm) with a ~10^2 increase in fluorescence intensity, confirming the fluorescence signature of HE oxidized in a $O_2^{\bullet-}$ dependent manner. **C)** HE (100 µM) separately measured in two reactions with a saturated potassium superoxide (KO_2) solution in 100% DMSO. (*Left*) a 100% DMSO solvent system, where the stable $O_2^{\bullet-}$ radical increases HE fluorescence (from red to black, increasing over 30 minutes), demonstrating 2-OH-E^+ formation. (*Right*) 50 mM phosphate buffer, pH 7.5, where the $O_2^{\bullet-}$ radical is highly unstable in a protic solvent, and rapidly disproportionates, demonstrating non-specific oxidation of HE to exhibit a red-shifted fluorescence (from red to black, increasing over 30 minutes).[2, 22]

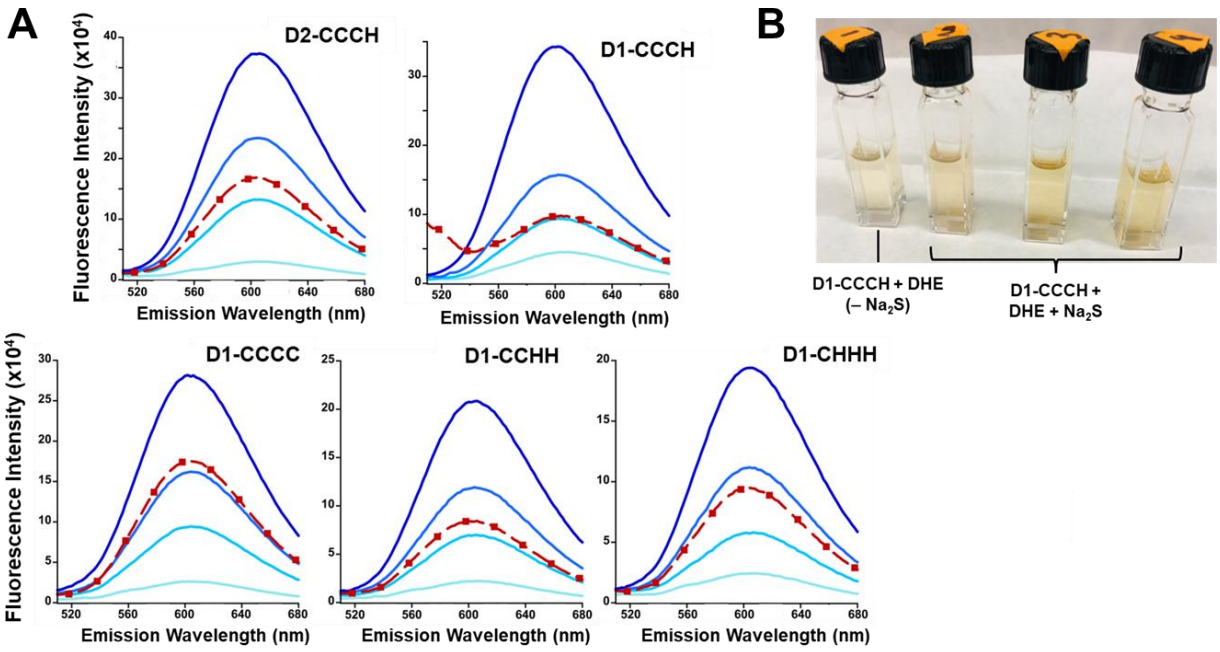

Figure S8. Fluorescence increases from hydroethidine (HE) oxidation by superoxide during TTP peptide persulfidation. A) Fluorescence increases over time (0, 30, 60, and 120 mins, from light to dark blue) from HE oxidation from superoxide during persulfidation of each TTP peptide. The dashed red line represents the fluorescence spectra at 120 mins of a control preparation for each variant omitting only Na_2S addition. **B)** TTP-D1 peptides exhibiting orange fluorescence 18 hours after initializing the reaction with Na_2S addition. Zn^{II}-loaded TTP peptides (20 μM Zn-TTP) were prepared in O_2-sparged phosphate buffer (50 mM, pH 7.5), scanned for initial fluorescence upon HE addition and for 2 hours following addition of Na_2S (2 mM Na_2S, 100-fold excess to protein).

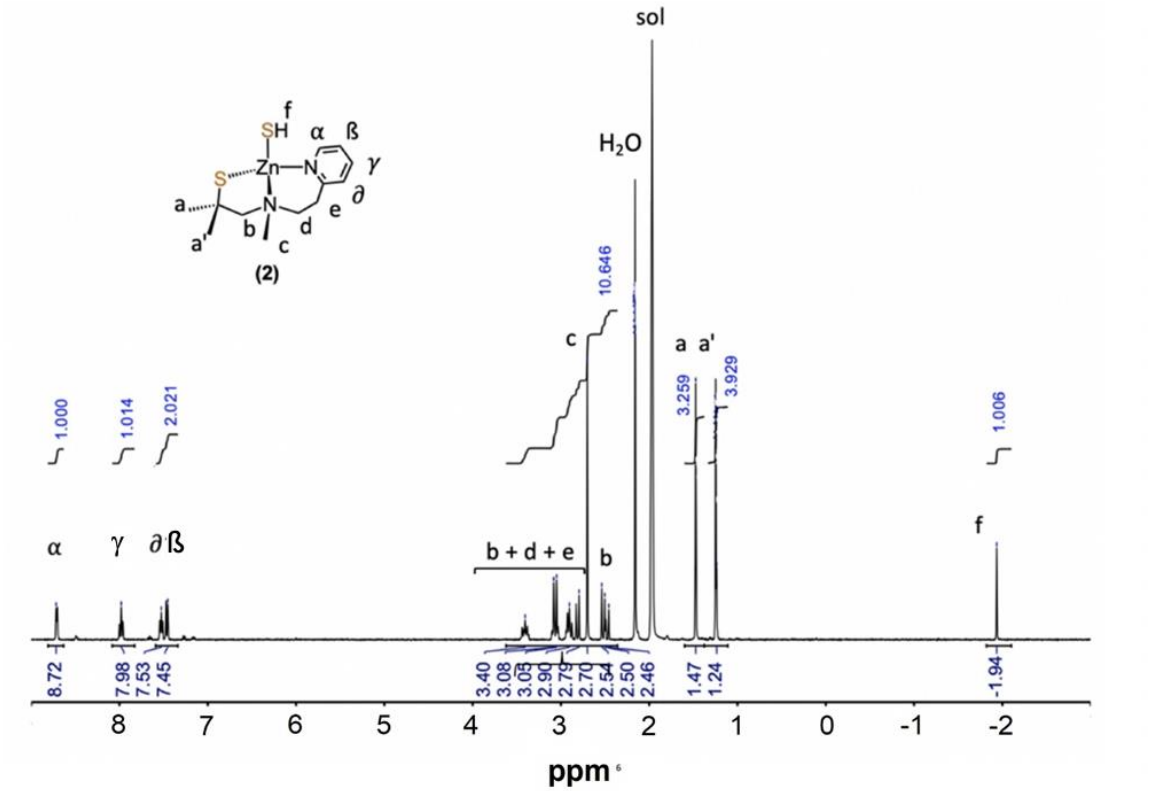

Figure S9. Characterization of Zn(PATH)(SH) by NMR spectroscopy. ^{1}H-NMR spectrum of Zn(PATH)(SH) (**2**) in CD_3CN (sol).

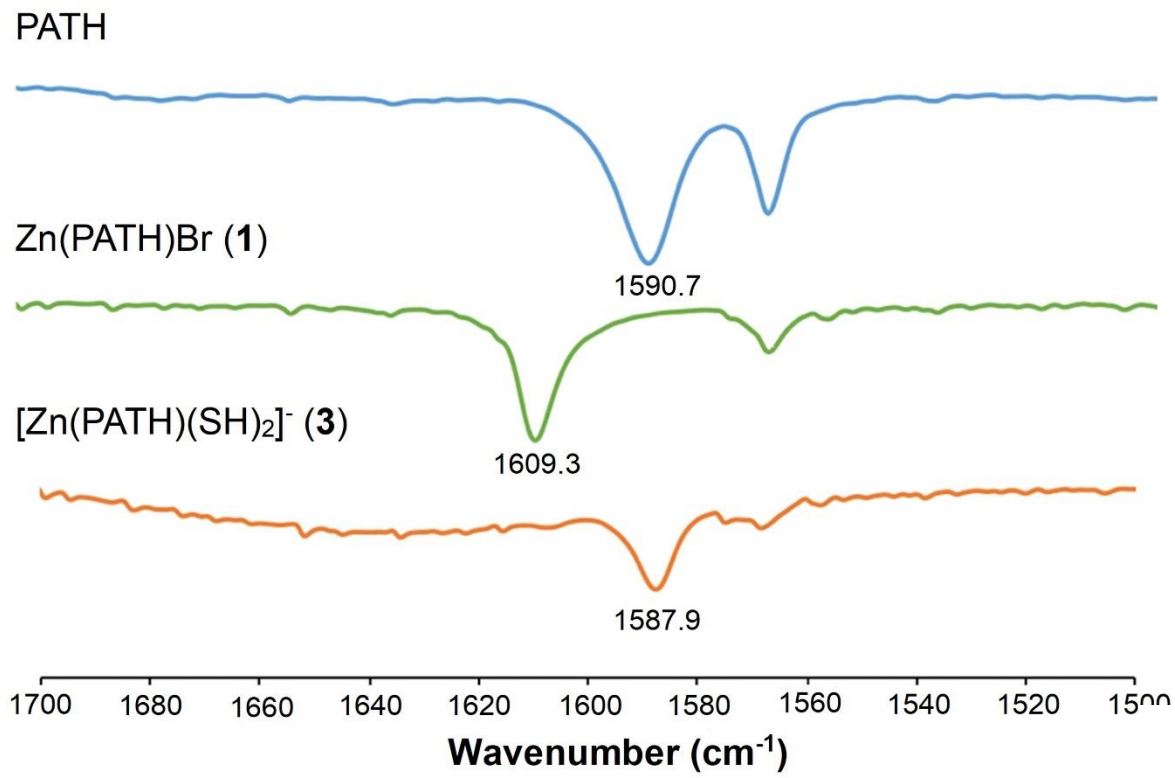

Figure S10. Comparison of FTIR spectra for PATH and its Zn^{II} complexes. PATH (blue line, top), Zn(PATH)Br (green line, middle), and $[Zn(PATH)(SH)_2]^-$ (orange line, bottom). Samples were dropcast as thin films with CH_3CN. The peaks marked at 1591 (top), 1609 (middle), and 1587 (bottom) cm^{-1} correspond to a pyridyl C=N stretching mode *(43)*.

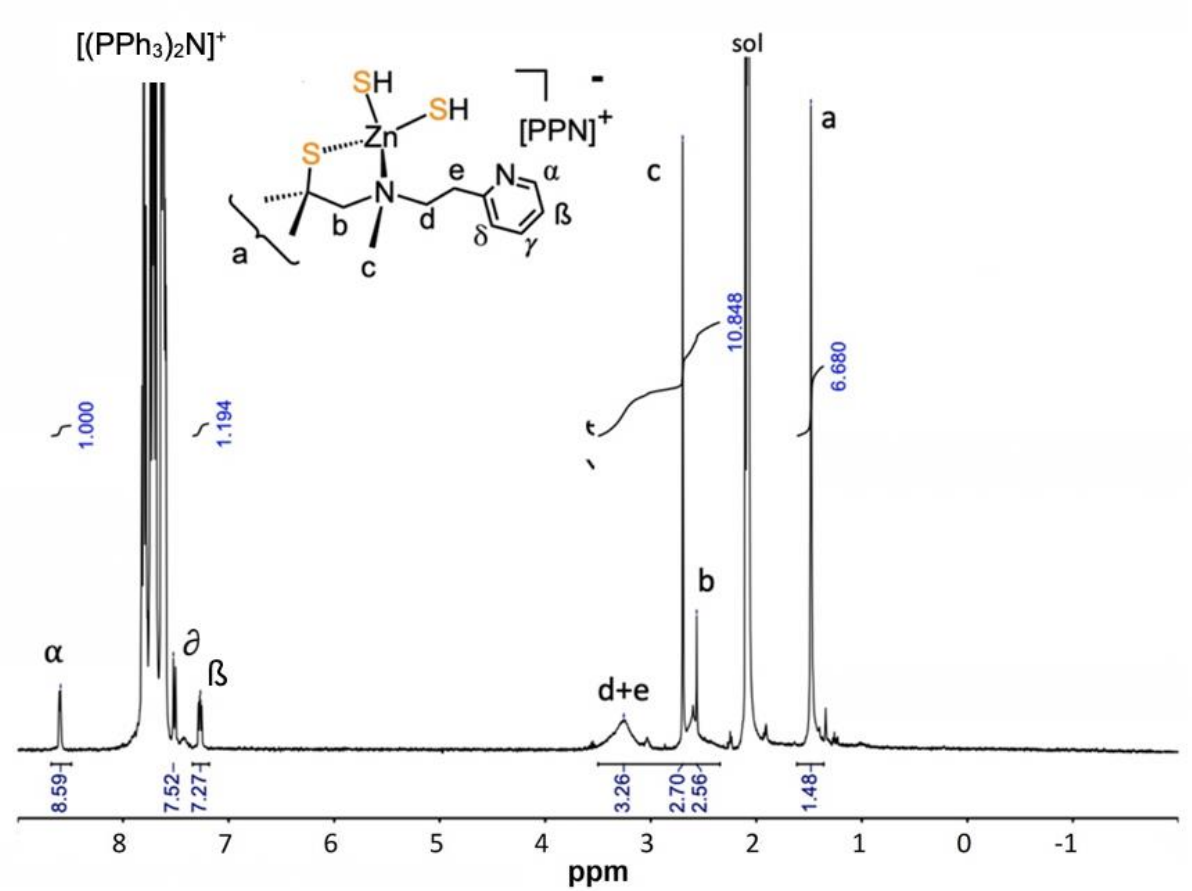

Figure S11. Characterization of $[Zn(PATH)(SH)_2]^-$ (3) by NMR spectroscopy. ^{1}H-NMR spectrum of **3** in CD_3CN (sol). Complex **3** was generated in solution from crystalline Zn(PATH)(SH) (**2**) by the addition of excess $[(PPh_3)_2N][SH]$. The peak corresponding to the pyridyl H_β proton is masked by peaks corresponding to the $[(PPh_3)_2N]^+$ cation. The peaks corresponding to the coordinated SH^- protons could not be assigned, likely due to rapid binding equilibria and/or SH exchange with free SH^-.

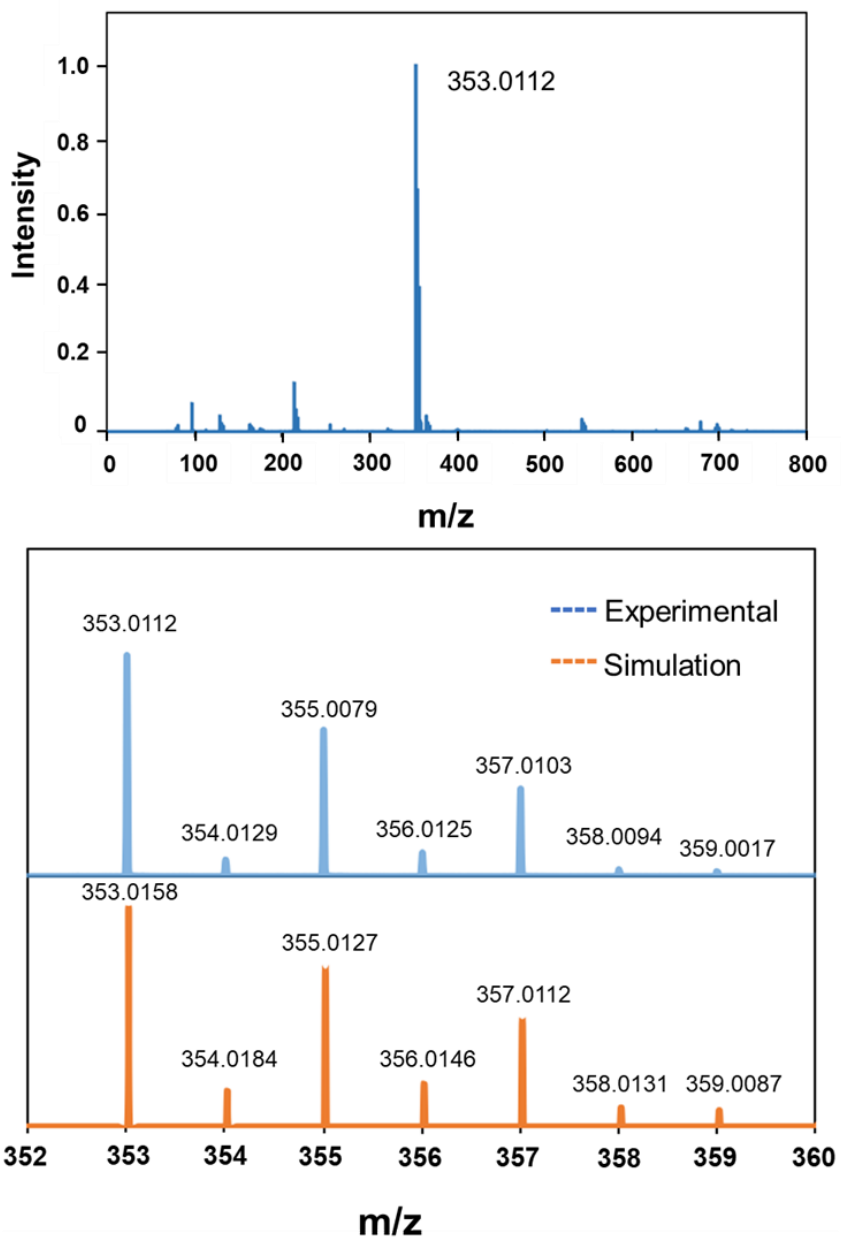

Figure S12. Characterization of $[Zn(PATH)(SH)_2]^-$ (3) by mass spectrometry. High resolution ESI-MS (negative ion mode) of $[Zn(PATH)(SH)_2]^-$ generated by addition of $[(PPh_3)_2N][SH]$ (2 equiv) to Zn(PATH)Br in CH_3CN (sol). Data for the range 0 – 800 *m/z*, showing an intense ion at 353.0112 (top), expanded region showing the isotopic cluster near the peak at 353.0112 *m/z* (middle), and calculated isotopic cluster for $C_{12}H_{21}N_2S_3Zn$ (bottom).

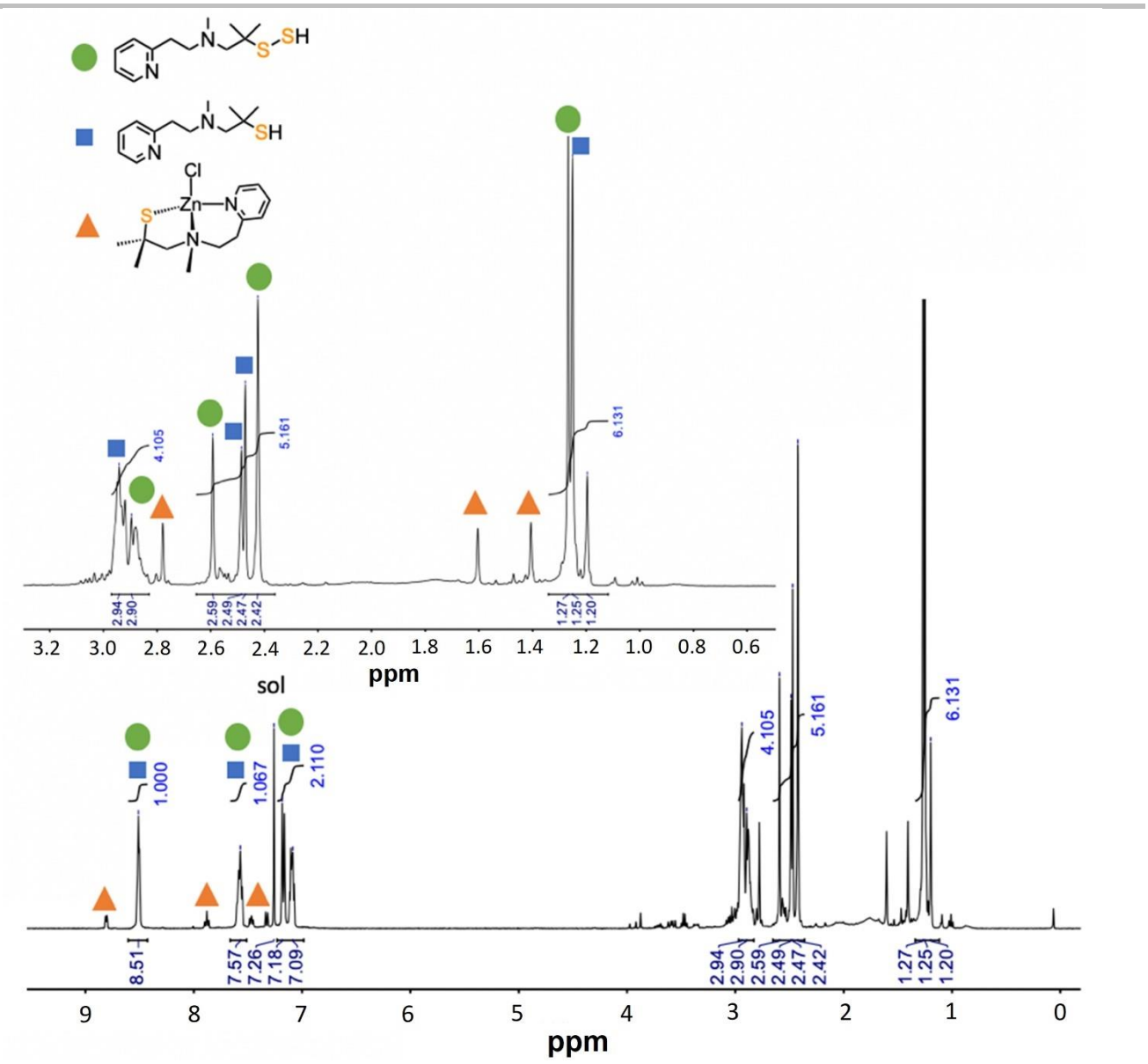

Figure S13. Characterization of persulfidated PATH by ^{1}H-NMR spectroscopy. ^{1}H-NMR spectrum ($CDCl_3$ (sol)) of the organic products isolated following the demetalation and workup of a reaction between Zn(PATH)Br, $[Bu_4N][SH]$ (3 equiv), and excess O_2 after 24 hours (see *synthetic procedures*). Persulfidated PATH (green circles), PATH (blue squares), Zn(PATH)Cl (orange triangles). *Inset:* Expanded alkyl region.

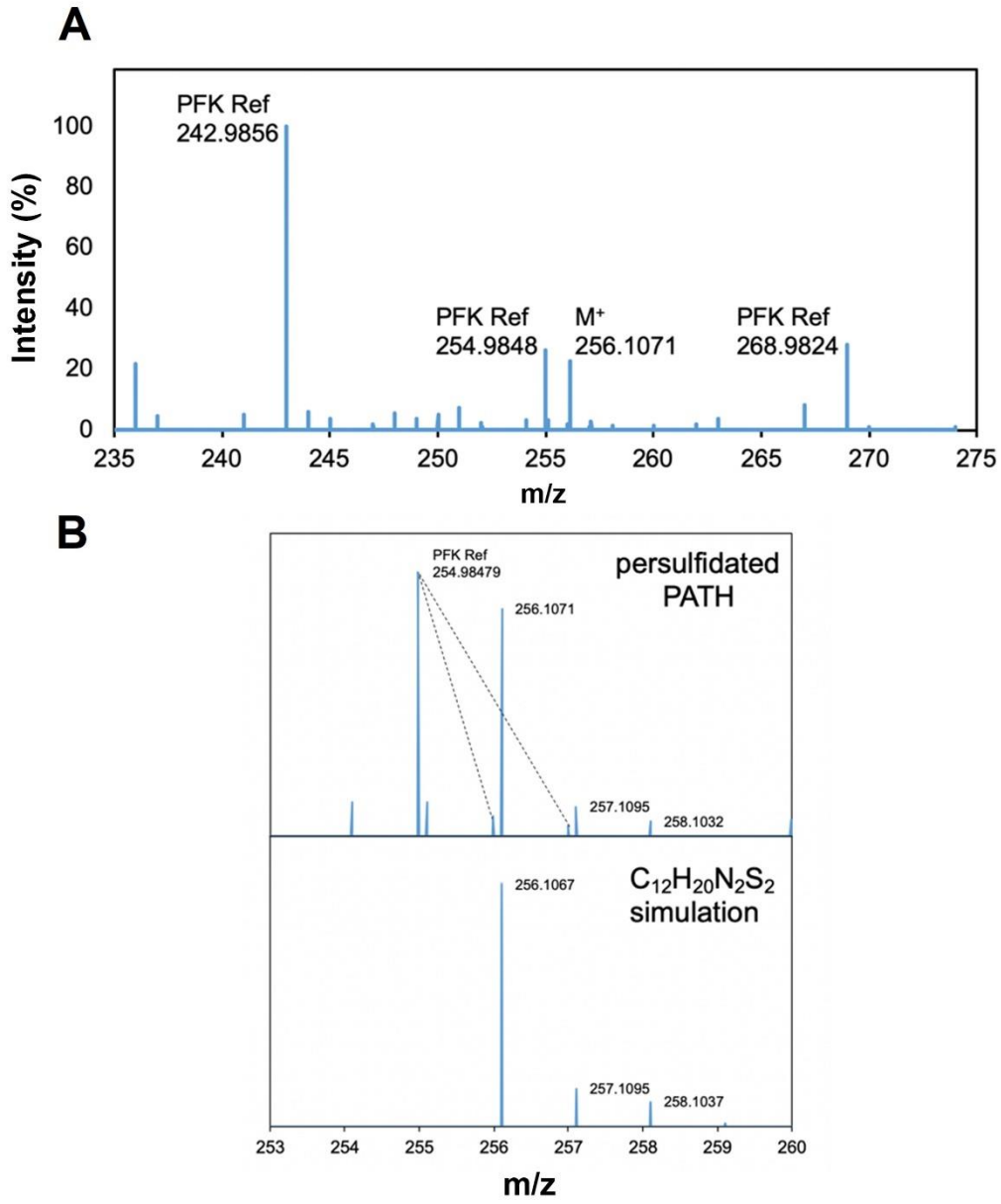

Figure S14. Characterization of persulfidated PATH by mass spectrometry. A) EI-MS of persulfidated PATH. Masses are referenced against a PFK internal standard. **B)** Expanded region showing the isotopic pattern near 256.1071 *m/z* (top) and calculated isotopic cluster for $C_{12}H_{20}N_2S_2$ (bottom).

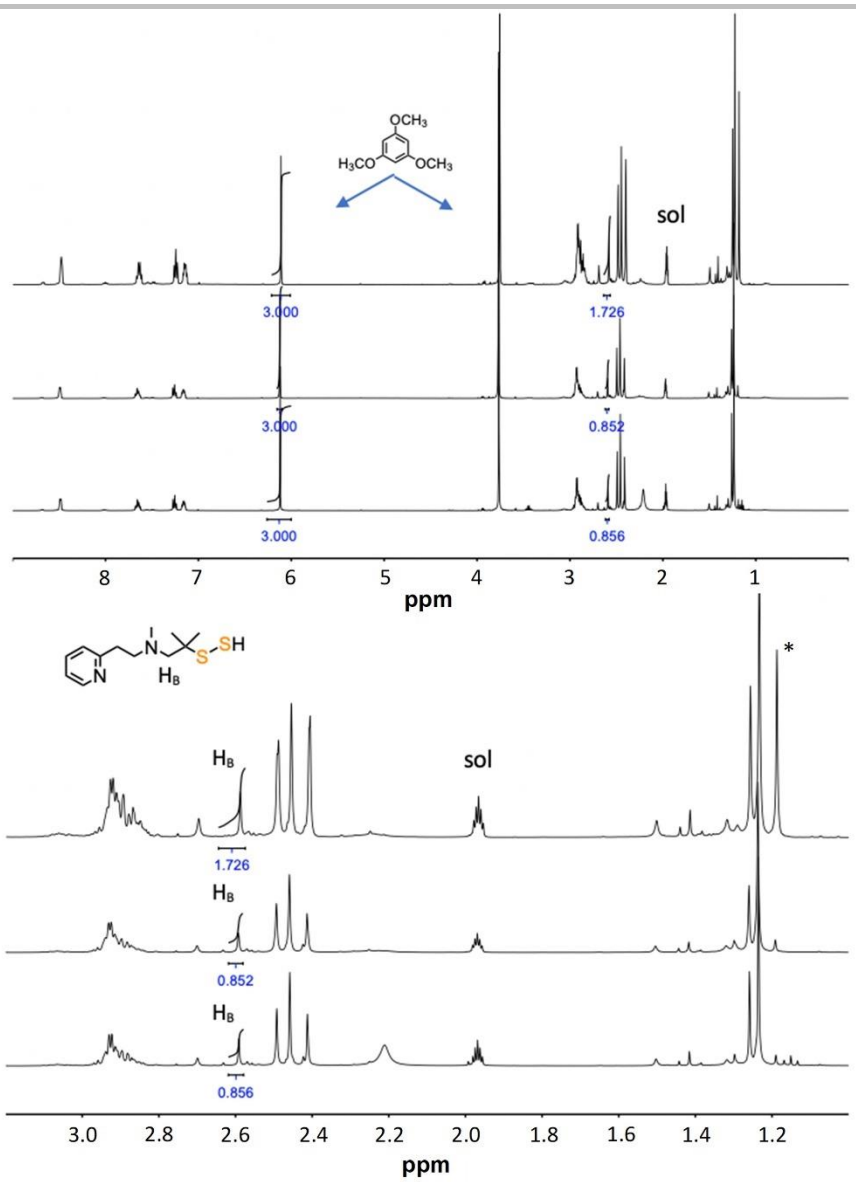

Figure S15. Quantitation of persulfidated PATH. ^{1}H-NMR spectra of the demetallation products following the reaction of $[Zn(PATH)(SH)_2]^-$ and O_2 (see *synthetic procedures*), showing persulfidated PATH and 1,3,5-trimethoxybenzene added as internal standard in CD_3CN (sol) (top), and expanded alkyl region (bottom). The peak assigned to H_B on the persulfidated PATH was integrated and compared with the integration of the aromatic protons of the standard at 6.12 ppm, giving a yield for persulfidated PATH of 11.8 ± 0.2%. Peak denoted with an asterisk corresponds to disulfide $(PATH)_2$ (*).

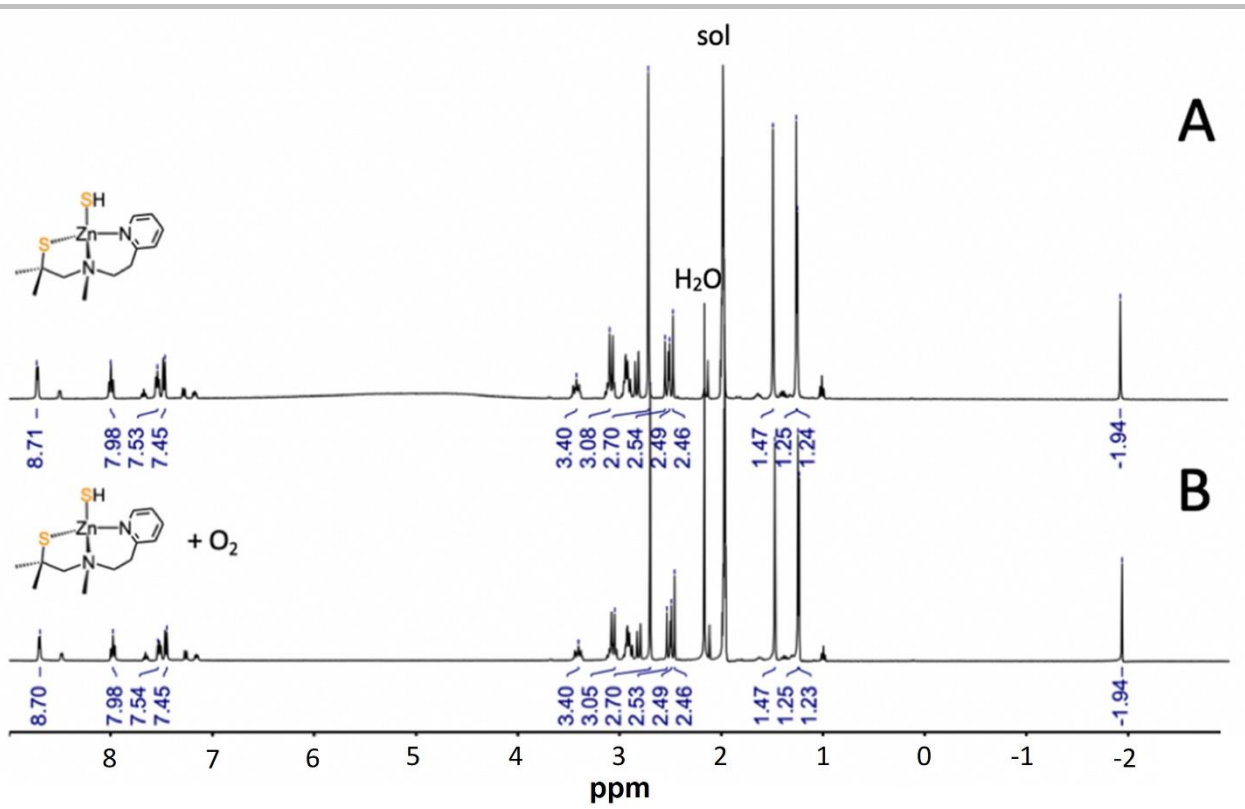

Figure S16. Control reaction of Zn(PATH)(SH) with O_2. A) ^{1}H-NMR spectrum of Zn(PATH)(SH) (**2**) in CD_3CN (sol) under anaerobic conditions. **B)** ^{1}H-NMR spectrum of Zn(PATH)(SH) (**2**) in CD_3CN (sol) 30 minutes after the addition of excess O_2, showing no change.

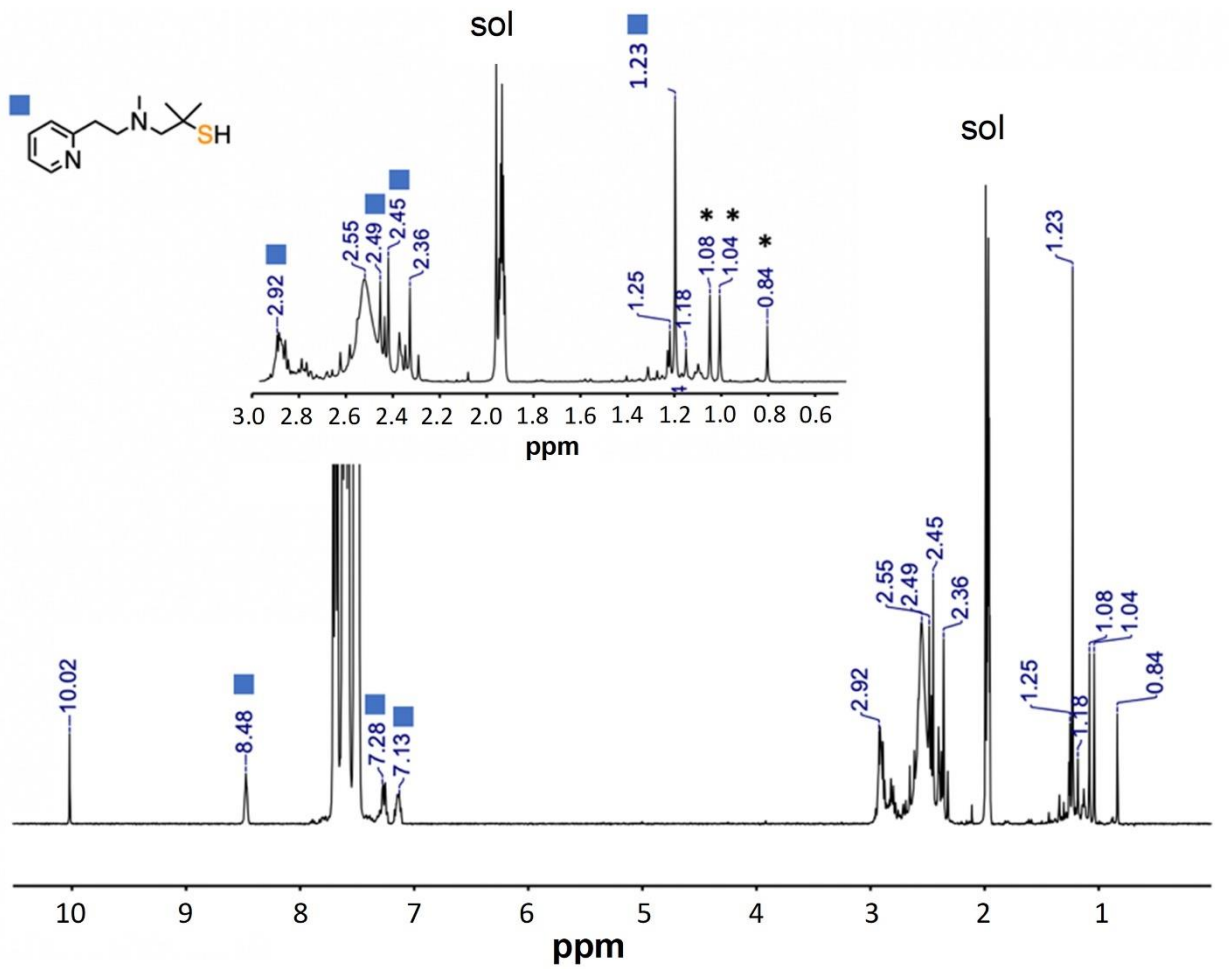

Figure S17. Control reaction of free ligand PATH with O_2 and $[(PPh_3)_2N][SH]$. ^{1}H-NMR spectrum of a reaction between PATH, excess O_2, and 3 equiv $[(PPh_3)_2N][SH]$ over the course of 180 minutes in CD_3CN (sol). Peaks corresponding to unreacted PATH are denoted with a blue square. Inset: expanded alkyl region. Unidentified products give rise to peaks marked with an asterisk (*). These peaks are distinct from PATH, disulfide $(PATH)_2$, or persulfidated PATH.

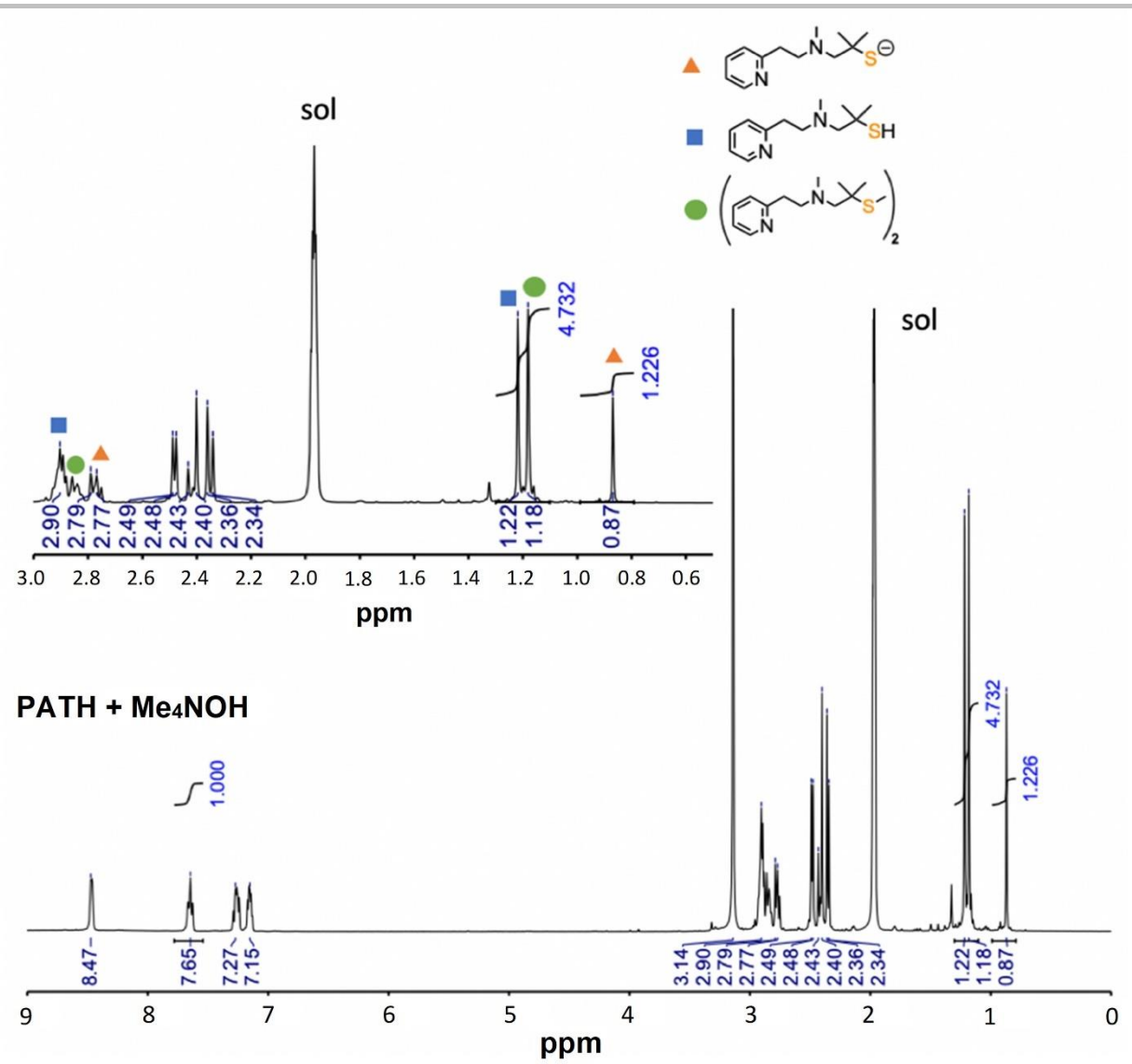

Figure S18. Control reaction of PATH and Me_4NOH. ^{1}H-NMR spectrum of the reaction of PATH in CD_3CN (sol) with excess base (Me_4NOH) in CD_3OD under aerobic conditions. The observed peaks are assigned to a mixture of PATH (blue squares), deprotonated PATH (orange triangle) and disulfide $(PATH)_2$ (green circle). *Inset:* Expanded alkyl region. No peaks for persulfidated PATH are observed.

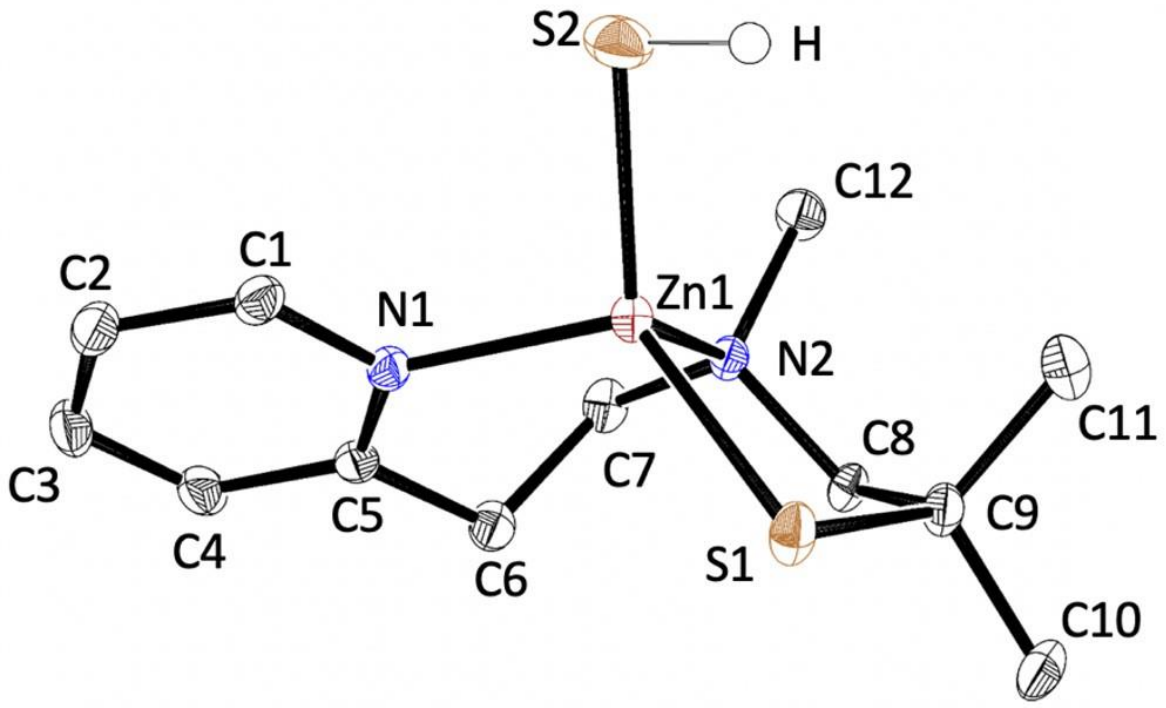

Figure S19. Displacement ellipsoid plot (50% probability level) for Zn(PATH)(SH) (2) at 110 K. Hydrogen atoms except for S-H have been omitted for clarity. Selected bond distances (Å): Zn1-N1, 2.0701(13); Zn1-N2, 2.1228(13); Zn1-S1, 2.2675(4); Zn1-S2, 2.2699(5); S2-H1, 1.17(2); selected bond angles (deg): N1-Zn1-S1, 117.82(4), N1-Zn1-S2, 102.47(4); N2-Zn1-S1, 91.64(4); N2-Zn1-S2, 117.81(4); N1-Zn1-N2, 98.02(5); Zn1-S2-H, 95.0(10).

References

[1] M. R. Filipovic, J. Zivanovic, B. Alvarez, R. Banerjee, *Chem. Rev.* **2018**, *118*, 1253-1337.

[2] K. R. Olson, *Free Radic. Biol. Med.* **2019**, *140*, 74-83.

[11a] M. Lange, K. Ok, G. D. Shimberg, B. Bursac, L. Markó, I. Ivanović‐Burmazović, S. L. J. Michel, M. R. Filipovic, *Angew. Chem. Int. Ed.* **2019**, *131*, 8081-8085.

[14b] J. Zivanovic, E. Kouroussis, J. B. Kohl, B. Adhikari, B. Bursac, S. Schott-Roux, D. Petrovic, J. L. Miljkovic, D. Thomas-Lopez, Y. Jung, M. Miler, S. Mitchell, V. Milosevic, J. E. Gomes, M. Benhar, B. Gonzalez-Zorn, I. Ivanovic-Burmazovic, R. Torregrossa, J. R. Mitchell, M. Whiteman, G. Schwarz, S. H. Snyder, B. D. Paul, K. S. Carroll, M. R. Filipovic, *Cell Metab.* **2019**, *30*, 1152-1170 e1113.

[15] L. Fu, K. Liu, J. He, C. Tian, X. Yu, J. Yang, *Antioxid. Redox Signal.* **2020**, *33*, 1061-1076.

[18] A. T. Stoltzfus, C. J. Campbell, M. M. Worth, K. Hom, T. L. Stemmler, S. L. J. Michel, *J. Biol. Inorg. Chem.* **2023**, *28*, 85-100.

[22] H. Zhao, S. Kalivendi, H. Zhang, J. Joseph, K. Nithipatikom, J. Vásquez-Vivar, B. Kalyanaraman, *Free Radic. Biol. and Med.* **2003**, *34*, 1359-1368.

[23] S. Chang, V. V. Karambelkar, R. C. diTargiani, D. P. Goldberg, *Inorg. Chem.* **2001**, *40*, 194-195.

[30] G. M. Sheldrick, *Acta. Crys.* **2015**, *71*, 3-8.

[31] a) B. Kalyanaraman, M. Hardy, R. Podsiadly, G. Cheng, J. Zielonka, *Arch. Biochem. Biophys.* **2017**, *617*, 38-47; bH. Zhao, S. Kalivendi, H. Zhang, J. Joseph, K. Nithipatikom, J. Vásquez-Vivar, B. Kalyanaraman, *Free Radic. Biol. and Med.* **2003**, *34*, 1359-1368.

Author Contributions

A.T.S., J.G.B., H.L., T.V., and S.L.J.M. designed experiments; A.T.S., J.G.B., H.L., T.V., M.M.W., L.M., M.A.S., and M.R.F. performed experiments; A.T.S., J.G.B., H.L., T.V., M.M.W., M.A.S., and S.L.J.M. analyzed data; A.T.S., J.G.B., H.L., M.R.F., D.P.G., and S.L.J.M. wrote and revised the paper; M.A.K., M.R.F., D.P.G., and S.L.J.M. supervised this project; and S.L.J.M. acquired funding for this project.